Physics of Plasmas ARTICLE scitation.org/journal/php

Equations and improved coefficients for parallel transport in multicomponent collisional plasmas: Method and application for tokamak modeling

Cite as: Phys. Plasmas **28**, 062308 (2021); doi: 10.1063/5.0047618
Submitted: 15 February 2021 · Accepted: 9 May 2021 ·
Published Online: 16 June 2021

View Online Export Citation CrossMark

S. O. Makarov,[1,a)] D. P. Coster,[1] V. A. Rozhansky,[2] A. A. Stepanenko,[3] V. M. Zhdanov,[3] E. G. Kaveeva,[2] I. Y. Senichenkov,[2] and X. Bonnin[4]

AFFILIATIONS

[1]Max-Planck-Institut für Plasmaphysik, D-85748 Garching, Germany
[2]Peter the Great St. Petersburg Polytechnic University, 195251 St. Petersburg, Russia
[3]National Research Nuclear University MEPhI (Moscow Engineering Physics Institute), Kashirskoe sh. 31, 115409 Moscow, Russia
[4]ITER Organization, CS 90 046, F-13067 St-Paul-Lez-Durance Cedex, France

[a)]**Author to whom correspondence should be addressed:** sergei.makarov@ipp.mpg.de

ABSTRACT

New analytical expressions for parallel transport coefficients in multicomponent collisional plasmas are presented in this paper. They are improved versions of the expressions written in Zhdanov [*Transport Processes in Multicomponent Plasma*, English ed. (Taylor and Francis, London, New York, 2002)], based on Grad's 21N-moment method. Both explicit and approximate approaches for the calculation of transport coefficients are considered. Accurate application of this closure for the Braginskii transport equations is discussed. Viscosity dependence on the heat flux is taken into account. Improved expressions are implemented into the SOLPS-ITER code and tested for deuterium and neon ITER cases. Some typos found in Zhdanov [*Transport Processes in Multicomponent Plasma*, English ed. (Taylor and Francis, London, New York, 2002)] are corrected.

I. INTRODUCTION

Fusion toroidal devices with magnetic confinement (tokamaks and stellarators) operate with multispecies plasma. Plasma composition can contain mixtures of main components: hydrogen, deuterium, tritium,[2] and helium isotopes; and impurities: helium, lithium, beryllium, carbon, nitrogen, neon, argon, etc.[3] (In some operational regimes, helium might be the main component and then, in addition to the usual impurities, isotopes of hydrogen would be impurities.) Edge plasmas usually are in a collisional regime, by which we mean that macroscopic parameters change slowly on parallel (perpendicular) length scales of the mean free path (gyroradius) and time scales between collisions (gyromotion period). Under this assumption, a closure method such as the one proposed by Braginskii[4] can be applied to the moments of the distribution function. However, this approach is applicable to the single ion species case and assumes only trace levels of impurities. For the multicomponent case, Grad's moment method[5] can be used. This method is based on the tensorial Hermite polynomials finite expansion approximation of the distribution function with a local Maxwellian distribution function as the zeroth-order approximation. It is developed in detail in Refs. 1 and 6. Transport equations for multicomponent fully ionized plasmas consisting of electrons and several species of ions each in a different charge state were obtained in the 21N-moment approximation by Zhdanov and Yushmanov (ZY).[6] The more complete set of moment equations, including equations for the partial viscous-stress tensors, is presented in Ref. 1. In this work, we study these equations to obtain improved versions of the expressions written in Ref. 1, though only parallel transport is considered in this paper. Equations for electrons can be solved separately due to the large electron–ion mass difference, as it was considered in Refs. 1 and 6. For ions, the situation is more complicated, especially for mixtures with comparable masses. This is analyzed in detail below.

Some previous work on implementing the moment approach can be found in Ref. 7 (based on Refs. 8 and 9 and described in Ref.

10) and Ref. 11 where an explicit implementation (based on matrix inversions) was implemented in SOLPS and EDGE2D; (Ref. 12) where the multispecies closure was implemented into 3D turbulence and transport codes based on Ref. 1; and additional work in Ref. 13. Some of this work assumed $m_{light}/m_{heavy} \ll 1$ and so could not be applied to deuterium, tritium, and helium mixture cases, while in others the closure for viscous-stress equations was not considered (or only the velocity-dependent part of the viscous stress tensors was taken into account). In addition, there is a difference between definitions chosen by Braginskii[4] and in Ref. 1. Thus, for the application of the closures discussed in Ref. 1 for the Braginskii equations, special corrections are developed in this paper (see Sec. II). Some typos in Ref. 1 which directly affect the results are corrected in Appendix C. In Refs. 7 and 11 a full closure (including equations for the viscous stress tensors) was implemented into the transport code, though the heat flux-dependent part of the viscous stress tensors was not considered and this effect plays an important role in toroidal systems.[14,15] Such a contribution from the viscous terms was added by Rozhansky *et al.*[16,17] for correct calculation of the radial electric field in the H-mode pedestal in tokamaks, but only in the single fluid case and can be extended to multispecies cases.

It is also valuable to mention the work Ref. 18, where Grad's moment method has been discussed and the temperatures of the main component and the impurity have been considered separately in the calculations of the Chapman–Cowling integrals, whereas in Refs. 1 and 6 and therefore in the present paper, the different temperatures have been kept only in the gradients in the collisional term. The impact of the impurity temperature deviation from the main component temperature in the Chapman–Cowling integrals on the impurity transport in the tokamak would be interesting to study.

In this paper, this generalization of the equation system is presented. Section II is dedicated to an accurate application of Grad's closure discussed in Ref. 1 for the Braginskii system of equations used in transport codes, for instance, SOLPS-ITER.[19,20] In addition, the heat flux-dependent part of the viscous stress tensors is considered in Sec. II.

Since the calculation of transport coefficients is supposed to be performed during the numerical solution of algebraic equations, this might be a problem in a fluid code where this would be done at each time step in each grid cell; therefore, new improved analytical expressions are developed in Sec. III. In the case where masses of species are significantly different, such methods can be applied. This method is an improvement over the method discussed in Refs. 1 and 6. Comparison for the improved expressions, the original expressions (8.4.7) in Ref. 1, and the solution of the explicit system of algebraic equations is provided. As it is shown there, even for the cases where masses of components are not too different, analytical formulas provide surprisingly good agreement with the explicit numerical approach. Moreover, for some cases, the new formulas provide a much better match with the numerical results than the original analytical expressions (8.4.7) in Ref. 1. The results can be found in Appendix A.

Then, in Sec. IV, a comparison between transport coefficients calculated using Grad's 21N-moment closure and transport coefficients used in the current SOLPS-ITER model is considered. Additionally, new expressions for thermal and friction forces were implemented into the SOLPS-ITER code and tested for neon transport in an ITER deuterium plasma and compared with the current SOLPS-ITER model.[21,22]

II. BASIC EQUATIONS FOR MULTISPECIES PLASMA

A. Equations

First of all, let us consider the system of fluid equations for species type α and charge state Z, which can be applied for both ions and electrons (for electrons $Z = -1$),

$$\partial_t n_{\alpha Z} + \nabla \cdot (\mathbf{u}_{\alpha Z} n_{\alpha Z}) = S^n_{\alpha Z}, \tag{1}$$

$$m_\alpha \partial_t (\mathbf{u}_{\alpha Z} n_{\alpha Z}) + \nabla \cdot \overleftrightarrow{\Gamma}^{m}_{\alpha Z} = -\nabla (n_{\alpha Z} T^{(Br)}_{\alpha Z}) + Z e n_{\alpha Z} (\mathbf{E} + [\mathbf{u}_{\alpha Z} \mathbf{B}]) - \nabla \cdot \overleftrightarrow{\pi}^{(Br)}_{\alpha Z} + \mathbf{R}_{\alpha Z} + \mathbf{S}^m_{\alpha Z}, \tag{2}$$

$$\frac{3}{2} \partial_t (n_{\alpha Z} T^{(Br)}_{\alpha Z}) + \nabla \cdot (\mathbf{q}^{(Br)}_{\alpha Z} + \frac{3}{2} \mathbf{u}_{\alpha Z} n_{\alpha Z} T^{(Br)}_{\alpha Z}) + n_{\alpha Z} T^{(Br)}_{\alpha Z} \nabla \cdot \mathbf{u}_{\alpha Z} = -((\overleftrightarrow{\pi}^{(Br)}_{\alpha Z} \nabla) \mathbf{u}_{\alpha Z}) + Q^{(Br)}_{\alpha Z} + S^E_{\alpha Z}. \tag{3}$$

Details can be found in Ref. 4. In this equation system, temperatures, heat fluxes, and viscosities are defined according to Braginskii,

$$n_{\alpha Z} = \iiint f_{\alpha Z} d^3\mathbf{v}, \quad n_{\alpha Z} u_{\alpha Z k} = \iiint v_k f_{\alpha Z} d^3\mathbf{v}, \tag{4}$$

$$T^{(Br)}_{\alpha Z} = \frac{2}{3} \frac{m_\alpha}{n_{\alpha Z}} \iiint \frac{(\mathbf{v} - \mathbf{u}_{\alpha Z})^2}{2} f_{\alpha Z} d^3\mathbf{v}, \tag{5}$$

$$q^{(Br)}_{\alpha Z k} = m_\alpha \iiint \frac{(\mathbf{v} - \mathbf{u}_{\alpha Z})^2}{2} (v_k - u_{\alpha Z k}) f_{\alpha Z} d^3\mathbf{v}, \tag{6}$$

$$\pi^{(Br)}_{\alpha Z k l} = m_\alpha \iiint \left[(v_k - u_{\alpha Z k})(v_l - u_{\alpha Z l}) - \frac{\delta_{kl}}{3} (\mathbf{v} - \mathbf{u}_{\alpha Z})^2 \right] f_{\alpha Z} d^3\mathbf{v}, \tag{7}$$

where $f_{\alpha Z}$ is the distribution function for ion or electron species αZ, k and l are component indices, and integrals of the collisional term $C_{\alpha Z}$ due to Coulomb (elastic) collisions provide

$$R_{\alpha Z k} = m_\alpha \iiint v_k C_{\alpha Z} d^3\mathbf{v}, \tag{8}$$

$$Q^{(Br)}_{\alpha Z} = m_\alpha \iiint \frac{(\mathbf{v} - \mathbf{u}_{\alpha Z})^2}{2} C_{\alpha Z} d^3\mathbf{v}. \tag{9}$$

Terms $S^n_{\alpha Z}$, $S^m_{\alpha Z i}$, $S^E_{\alpha Z}$ describe, respectively, particle, momentum, and energy sources due to inelastic collisions between charged species (ionization, recombination, and excitation) and all interactions with neutrals, and they are considered as external parameters in this model. For instance, in SOLPS-ITER these sources are calculated by the EIRENE code.[23] Moreover, since in the approach, discussed in the present paper, the collision operator is considered in the Boltzmann form, inelastic collisions can be computed internally by moment treatment of the neutral particles, details can be found in Refs. 24 and 25.

The momentum flux due to the flow velocity is

$$\Gamma^m_{\alpha Z k l} = m_\alpha u_{\alpha Z k} u_{\alpha Z l} n_{\alpha Z}. \tag{10}$$

In a multispecies plasma, the transport coefficients, which help to express $\mathbf{q}^{(Br)}_{\alpha Z}$, $\overleftrightarrow{\pi}^{(Br)}_{\alpha Z}$, $\mathbf{R}_{\alpha Z i}$, and $Q^{(Br)}_{\alpha Z}$ through densities, velocities, temperatures, and their spatial derivatives, differ significantly for different

plasma species, different species densities, and different mass ratios of species. This means that no simplification may be made in the general case, and general methods for the solution of kinetic equations should be used.

Such a method is Grad's 21N-moment method, described in Ref. 1. Following Ref. 1, we define

$$T_{\alpha Z} = \frac{2}{3}\frac{m_\alpha}{n_{\alpha Z}}\int\int\int \frac{(\mathbf{v}-\mathbf{u})^2}{2} f_{\alpha Z} d^3\mathbf{v}, \tag{11}$$

$$h_{\alpha Zk} = m_\alpha \int\int\int \frac{(\mathbf{v}-\mathbf{u})^2}{2}(v_k - u_k) f_{\alpha Z} d^3\mathbf{v} - \frac{5}{2} w_{\alpha Zk} n_{\alpha Z} T_{\alpha Z}, \tag{12}$$

$$\pi_{\alpha Zkl} = m_\alpha \int\int\int \left[(v_k - u_k)(v_l - u_l) - \frac{\delta_{kl}}{3}(\mathbf{v}-\mathbf{u})^2\right] f_{\alpha Z} d^3\mathbf{v}, \tag{13}$$

where

$$\mathbf{w}_{\alpha Z} = \mathbf{u}_{\alpha Z} - \mathbf{u}; \quad \mathbf{u} = \frac{\sum_{\alpha,Z} m_\alpha n_{\alpha Z}\mathbf{u}_{\alpha Z}}{\sum_{\alpha,Z} m_\alpha n_{\alpha Z}}. \tag{14}$$

One can note that temperature (11), heat flux (12), and the viscous stress tensor (13) are defined in Ref. 1 with respect to the mass-averaged flow velocity (14), while (5)–(7) are defined with respect to the flow velocity of the corresponding species. Note that the temperature definition (5) is the standard fluid temperature definition, and it is not specific only to the Braginskii method, the superscript (*Br*) is only meant to distinguish between (5) and (11). Definitions (11)–(13) are more suitable for this method; therefore, they were used in Ref. 1. Thus, the result of the closure discussed in Ref. 1, that is expressed in the heat flux, viscosity, friction term, and heat exchange term, can be applied for the Braginskii system of equations (1)–(3) using corrections due to difference in definitions.

Indeed,

$$T_{\alpha Z} = T_{\alpha Z}^{(Br)} + \frac{1}{3} m_\alpha \mathbf{w}_{\alpha Z}^2, \tag{15}$$

$$q_{\alpha Zk}^{(Br)} = h_{\alpha Zk} + n_{\alpha Z} w_{\alpha Zk} m_\alpha \mathbf{w}_{\alpha Z}^2 - \sum_s w_{\alpha Zs}\pi_{\alpha Zsk}, \tag{16}$$

$$\pi_{\alpha Zkl}^{(Br)} = \pi_{\alpha Zkl} - m_\alpha n_{\alpha Z} w_{\alpha Zk} w_{\alpha Zl} + m_\alpha n_{\alpha Z}\frac{\delta_{kl}}{3}\mathbf{w}_{\alpha Z}^2. \tag{17}$$

A similar correction should be applied to the heat exchange term,

$$Q_{\alpha Z}^{(Br)} = Q_{\alpha Z} - \mathbf{w}_{\alpha Z}\cdot\mathbf{R}_{\alpha Z}, \tag{18}$$

where according to Ref. 1,

$$Q_{\alpha Z} \equiv m_\alpha \int\int\int \frac{(\mathbf{v}-\mathbf{u})^2}{2} C_{\alpha Z} d^3\mathbf{v} = -3\sum_{\beta,\zeta}\left(\frac{\mu_{\alpha\beta}}{m_\alpha + m_\beta}\right)\frac{n_{\alpha Z}}{\tau_{\alpha Z\beta\zeta}^{(Zh)}}(T_{\alpha Z} - T_{\beta\zeta}), \tag{19}$$

where summation is performed over all species and the definition of the collision time can be found in Appendix A. One can recognize a heat source due to friction between different ions in the second term of (18).

The friction term $\mathbf{R}_{\alpha Z}$ defined according to (8) does not need correction provided that Coulomb collisions do not lead to particle sources and sinks and three possible definitions are equivalent,

$$m_\alpha \int\int\int (\mathbf{v}-\mathbf{u}_{\alpha Z}) C_{\alpha Z} d^3\mathbf{v} = m_\alpha \int\int\int (\mathbf{v}-\mathbf{u}) C_{\alpha Z} d^3\mathbf{v} = \mathbf{R}_{\alpha Z}. \tag{20}$$

Therefore, the friction term $\mathbf{R}_{\alpha Z}$ found using the approach discussed in Ref. 1 may be directly substituted into the system (1)–(3).

Note, according to Eq. (8.1.3) in Ref. 1, that momentum conservation in collisions is maintained,

$$\sum_{\alpha,Z}\mathbf{R}_{\alpha Z} = 0. \tag{21}$$

So is energy conservation according to (18),

$$\sum_{\alpha,Z} Q_{\alpha Z}^{(Br)} = -\sum_{\alpha,Z}\mathbf{u}_{\alpha Z}\cdot\mathbf{R}_{\alpha Z}. \tag{22}$$

Details about the conservative property of collisions can be found, for instance, in Ref. 4.

Consecutively, Eq. (18) is necessary to maintain energy conservation. Also, here we note that the corrections (15)–(17) can be the same order as second order collisional terms, which are neglected in the method.[1] Therefore, when the corrections contribute significantly, one should carefully examine the method's limitations. Let us discuss an example, where the species "αZ" does not contribute significantly to the mass-average velocity (14), while the species "$\beta\zeta$" provide the main contribution to the mass-average velocity (14). Then, the mass-average velocity is close to the flow velocity of species $\beta\zeta$. Therefore, $\mathbf{w}_{\alpha Z}^2 \gg |\mathbf{w}_{\beta\zeta}|\cdot|\mathbf{w}_{\alpha Z}|$. In this case, when the corrections by the order of $\mathbf{w}_{\alpha Z}^2$ and $|\mathbf{w}_{\alpha Z}|\cdot\mathbf{w}_{\alpha Z}^2$ become important for the moments of species αZ (15)–(17), the second order term in the collisional term, which is by the order of $\frac{|\mathbf{w}_{\beta\zeta}|\cdot|\mathbf{w}_{\alpha Z}|}{\sqrt{T_{\beta\zeta}/m_\beta}\cdot\sqrt{T_{\alpha Z}/m_\alpha}}$, remains small. In the case, where $|\mathbf{w}_{\beta\zeta}|\cdot|\mathbf{w}_{\alpha Z}|$ become comparable to $\sqrt{T_{\beta\zeta}/m_\beta}\cdot\sqrt{T_{\alpha Z}/m_\alpha}$, next order terms in the collisional r.h.s. have to be considered.

Thus, assuming that the 21N-moment method is applied and transport coefficients are found, we need then to switch from $\mathbf{h}_{\alpha Z}$ and $\overleftrightarrow{\pi}_{\alpha Z}$ to $\mathbf{q}_{\alpha Z}^{(Br)}$ and $\overleftrightarrow{\pi}_{\alpha Z}^{(Br)}$ by using (16), (17) and taking into account the connection between temperatures (15).

In the present paper, we consider only so-called parallel (with regard to the B-field) transport coefficients. The classical transport across the magnetic field is usually of little consequence for magnetic fusion devices, since the anomalous transport is in most cases much larger.

Then, as it is shown in Ref. 1, the transport coefficients appearing in the heat flux and friction force may be calculated independently of the viscosity coefficients. Therefore, we may consider their corresponding calculations separately.

Finally, this approach can be applied both for electrons and ions. However, due to the small electron–ion mass ratio, transport for electrons can be considered separately, which significantly simplifies the approach. It is discussed in detail in Ref. 1. Also, we mention here that the electron heat conductivity, the velocity-dependent electron heat flux, and the thermal and friction forces have been implemented into the SOLPS-ITER code earlier[21,22,26] using this approach Ref. 1. Consequently, all the analysis in this paper will be devoted to ion transport coefficients.

B. Heat flux and friction term

Applying Grad's 21N-moment method (see Refs. 1 and 6, one can express $\mathbf{h}_{\alpha Z}$ through the velocities $\mathbf{w}_{\alpha Z}$ and temperature gradients

$\nabla T_{\alpha Z}$ with the help of kinetic coefficients that can be found solving, e.g., the algebraic system of equations (8.4.2) in Ref. 1. For the parallel (with regard to the B-field) component of $\mathbf{h}_{\alpha Z}$, one gets [see Eq. (8.4.6) of Ref. 1]

$$h_{\alpha Z\|} = -\frac{n_{\alpha Z}}{n_\alpha}\sum_\beta\left[\widetilde{c}^{(h_T^A)}_{\beta\alpha}\frac{n_\beta T}{m_\beta}\tau^{(Zh)}_{\beta\alpha}\widetilde{\nabla_\| T_\beta}\right] - 2c^{(h_T^B)}_\alpha\frac{n_{\alpha Z}T}{m_\alpha}\tau^{(Zh)}_{\alpha\alpha}\frac{\overline{Z^2_\alpha}}{Z^2}\nabla_\| T_{\alpha Z} + n_{\alpha Z}T\sum_\beta c^{(h_w)}_{\beta\alpha}(w_{\alpha Z\|} - \bar{w}_{\beta\|}), \tag{23}$$

where $\nabla_\| = (\mathbf{b}\cdot\nabla)$, and summation is performed over all types of ions and

$$\widetilde{\nabla_\| T_\alpha} = \sum_Z \frac{n_{\alpha Z}}{n_\alpha}\nabla_\| T_{\alpha Z}. \tag{24}$$

Collisional times $\tau^{(Zh)}_{\beta\alpha}$ and average squared charge $\overline{Z^2_\alpha}$ can be found in Appendix A. Kinetic coefficients $\widetilde{c}^{(h_T^A)}_{\beta\alpha}$, $c^{(h_w)}_{\beta\alpha}$ and $c^{(h_T^B)}_\alpha$ are the result of solving the system of algebraic equations (8.4.2) in Ref. 1 and application of corrections for each charge state (details can be found in Appendix A).

Note that the first two terms on the r.h.s. of (23) represent the thermal conductivity. The third term is the velocity difference dependent part of the heat flux, which is an additional contribution besides the thermal conductivity, and is not presented in the single ion species approaches.

Then, following the method in Refs. 1 and 6, the friction term can be written in the same form as Eq. (8.4.5) of Ref. 1,

$$R_{\alpha Z\|} = -n_{\alpha Z}\frac{Z^2}{\overline{Z^2_\alpha}}\sum_\beta\widetilde{c}^{(R_T^A)}_{\alpha\beta}\widetilde{\nabla_\| T_\beta} - n_{\alpha Z}c^{(R_T^B)}_\alpha\nabla_\| T_{\alpha Z} - n_{\alpha Z}\frac{Z^2}{\overline{Z^2_\alpha}}\sum_\beta\frac{\mu_{\alpha\beta}}{\tau^{(Zh)}_{\alpha\beta}}c^{(R_w)}_{\beta\alpha}(w_{\alpha Z\|} - \bar{w}_{\beta\|}), \tag{25}$$

where coefficients $\widetilde{c}^{(R_T^A)}_{\beta\alpha}$, $c^{(R_w)}_{\beta\alpha}$, and $c^{(R_T^B)}_\alpha$ are the result of solving the system of algebraic equations (8.4.2) in Ref. 1 and application of corrections for each charge state as well. In (25), the first two terms represent the thermal force, and the third term is the interspecies friction force.

C. Viscous stress tensor

Now let us consider the system of equations for viscous stress tensors. Note that, to describe parallel transport correctly Ref. 14 and references therein), it is required to take into account the heat flux dependence for the viscous stress tensors. However, this effect was not considered in the viscous stress tensor equations (8.1.6) and (8.1.6') in Ref. 1. The necessity to account for this heat viscosity requires a modification of the approach described in Ref. 1, namely, using the general expression for the moment equation (A1.8) in Ref. 1 and adding the heat flux-dependent terms to the left-hand side of (8.1.6) and (8.1.6') in Ref. 1 (after summation over charge states),

$$p_\alpha W_{|||} + W^{\bar{h}_\alpha}_{|||} = \bar{R}^{20}_{\alpha|||}, \tag{26}$$

where $\bar{R}^{20}_{\alpha|||}$ is the collisional right-hand side of Eq. (8.1.6) in Ref. 1 summed over charge states, that depends on $\bar{\pi}_{\beta|||}$ (β represents each ion in the mixture), and

$$\frac{7}{2}\frac{T}{m_\alpha}W^{\bar{h}_\alpha}_{|||} = \bar{R}^{21}_{\alpha|||}, \tag{27}$$

where $\bar{R}^{21}_{\alpha|||}$ is the collisional right-hand side of Eq. (8.1.6') in Ref. 1 summed over charge states, which also depends on $\bar{\pi}_{\beta|||}$.

W-tensors and collisional right-hand sides can be found in Appendix A. The solution of this system of equations (26) and (27) can be expressed as

$$\pi_{\alpha Z|||} = -\frac{n_{\alpha Z}}{n_\alpha}\left(\sum_\beta\left[\widetilde{c}^{(\pi_u^A)}_{\alpha\beta} + 2c^{(\pi_u^B)}_\alpha\frac{\overline{Z^2_\alpha}}{Z^2}\delta_{\alpha\beta}\right]\tau^{(Zh)}_{\beta\alpha}p_\beta\right)W_{|||} - \frac{n_{\alpha Z}}{n_\alpha}\sum_\beta\left(\widetilde{c}^{(\pi_h^A)}_{\alpha\beta}\tau^{(Zh)}_{\beta\alpha}W^{\bar{h}_\beta}_{|||}\right) - 2c^{(\pi_h^B)}_\alpha\frac{\overline{Z^2_\alpha}}{Z^2}\tau^{(Zh)}_{\alpha\alpha}W^{h_{\alpha Z}}_{|||}, \tag{28}$$

where dimensionless transport coefficients $\widetilde{c}^{(\pi_u^A)}_{\alpha\beta}$, $\widetilde{c}^{(\pi_h^A)}_{\alpha\beta}$ are the result of solving the system of algebraic equations (26) and (27), and the corrections for each charge state $c^{(\pi_u^B)}_\alpha$, $c^{(\pi_h^B)}_\alpha$ can be found analytically, as it is done for the heat flux (see Appendix A). The first term in (28) is the velocity-dependent part of the viscous stress tensor that is discussed in Ref. 1. The last terms in (28) represent additional effects due to the heat flux that is taken into account in this paper by adding heat flux-dependent terms into the left-hand side both in (26) and (27).

Usually, it is not a trivial task in complex geometry to take a divergence, such as $\nabla\cdot\bar{\pi}_{\alpha Z}$, intended to be included into (2), even in case (28). One way to do it supposes to take into account only parallel and drift components of the velocity and parallel and diamagnetic components of the heat flux in the viscous stress tensor calculation. Details can be found in Appendix B.

Finally, to apply the closure discussed in Ref. 1 and in this paper for the Braginskii system of equations (1)–(3), corrections of temperatures, heat fluxes, and viscosities should be done according to (15)–(17).

Now, let us recall the results of transport in the Pfirsch–Schlüter regime.[14,15,27,28] It is important to mention that, in the Pfirsch–Schlüter regime, where the collision frequency is larger than the bounce frequency,[15] the parallel transport coefficients can be calculated locally, as it is done in the present paper. Thus, it can be compared with the results of flux-surface average approaches,[15,27] where the parameters are not changing significantly on the magnetic surface. Local coefficients are supposed to be added into the 2D code, which describe the transport close to the separatrix, where the flux-averaged approach is not applicable. Moreover, in Refs. 15 and 27 the collision operator was used in the Fokker–Planck form, while the current approach[1] is based on the Boltzmann form collision operator, which can be more accurate in the high collisionality regime. It is necessary to note that, using the moment approach following the Braginskii-like method, one can also reproduce results in the Pfirsch–Schlüter regime.[14,29] In the single ion species case, one can calculate viscosity transport coefficients using (28) as well. Thus, using the notation from Ref. 14, they are

$$\mu_{\alpha 1} = p_i 2\tau^{(Zh)}_{ii}\times 0.96, \quad \mu_{\alpha 2} = p_i 2\tau^{(Zh)}_{ii}\times 1.55. \tag{29}$$

That is close to what was obtained in Refs. 14 and 15 and applied in Refs. 16 and 17 Therefore, in the collisional case, it is expected to obtain a radial electric field close to the radial electric field in the Pfirsch–Schlüter regime.[27] It is important to mention that to get $\mu_{\alpha 2}$ as in (29), it is necessary to add the heat flux-dependent term both into (26) and (27). Note that, using a moment approach for the single ion plasma,[29] that result (29) can be also obtained, and now, using the Grad's 21N-moment method, it is extended to arbitrary plasma mixtures.

D. Summary

In this section, we have considered an explicit method based on solving an algebraic system of equations, which can be applied for various plasma compositions, for example, deuterium, tritium, helium, and other impurities. This case occurs in current devices[30] and will be standard operating procedure in future reactors.[31–33] Thus, it should be implemented into codes like SOLPS-ITER,[19,20] which are used for fusion reactor operation predictions. Section IV is dedicated to this.

In Sec. III, an analytical approach is considered, which can be applied for many cases and which is, however, less accurate for species with close masses.

III. IMPROVED ANALYTICAL EXPRESSIONS

A. Heat flux

Let us consider the closure in the case with one light and several heavy ion species. The resulting $2n_s \times 2n_s$ matrix [where n_s is the number of different types of species (which have different atomic nuclei) in a mixture], which is intended to be inverted to solve the system of equations (8.4.2) in Ref. 1, can be split into blocks,

$$A = \begin{bmatrix} A_{11} & A_{12} \\ A_{21} & A_{22} \end{bmatrix}, \quad A^{-1} = \begin{bmatrix} \widetilde{A}_{11} & \widetilde{A}_{12} \\ \widetilde{A}_{21} & \widetilde{A}_{22} \end{bmatrix}, \tag{30}$$

where each block can be written

$$A_{qp} = \begin{bmatrix} a_{00}^{qp} & a_{01}^{qp} & \cdots & a_{0n_s}^{qp} \\ a_{10}^{qp} & a_{11}^{qp} & \cdots & a_{1n_s}^{qp} \\ \vdots & \vdots & \ddots & \vdots \\ a_{n_s0}^{qp} & a_{n_s1}^{qp} & \cdots & a_{n_sn_s}^{qp} \end{bmatrix}, \quad \widetilde{A}_{qp} = \begin{bmatrix} \widetilde{a}_{00}^{qp} & \widetilde{a}_{01}^{qp} & \cdots & \widetilde{a}_{0n_s}^{qp} \\ \widetilde{a}_{10}^{qp} & \widetilde{a}_{11}^{qp} & \cdots & \widetilde{a}_{1n_s}^{qp} \\ \vdots & \vdots & \ddots & \vdots \\ \widetilde{a}_{n_s0}^{qp} & \widetilde{a}_{n_s1}^{qp} & \cdots & \widetilde{a}_{n_sn_s}^{qp} \end{bmatrix}. \tag{31}$$

Here and further, index 0 represents the light species, while indices $1..n_s$ correspond to heavy species. Indices $q = 1, 2$ and $p = 1, 2$ refer to the corresponding blocks. Note that in the codes, which are applied for light main ion and heavy impurities,[19] main and impurity species are usually explicitly specified, and equations for them are written differently. The approach discussed in this paper allows us to write equations uniformly for all species.

First of all, for the diagonal elements, estimations can be made ($i \neq 0$),

$$\frac{a_{00}^{qp}}{a_{0i}^{qp}} \propto \frac{m_i}{m_0} \sum_{\beta=0..n_s} \frac{\overline{Z_\beta^2} n_\beta}{\overline{Z_i^2} n_i}, \tag{32}$$

$$A_{11}, A_{12} : a_{0i}^{1p} = a_{i0}^{1p}, \quad A_{21}, A_{22} : \frac{a_{0i}^{2p}}{a_{i0}^{2p}} \propto \frac{m_i}{m_0}. \tag{33}$$

Taking into account that $\sum_{\beta=0..n_s} \frac{\overline{Z_\beta^2} n_\beta}{\overline{Z_i^2} n_i} \geq 1$, cross elements in the first row and column are smaller than a_{00}^{qp} by at least the mass ratio. Thus, $\widetilde{a}_{00}^{qp}$ elements of the inverted matrix can be obtained independently from the contributions due to heavy species in the cross elements and $\widetilde{a}_{00}^{qp} \gg \widetilde{a}_{0i}^{qp}$.

Consider the solution for the temperature-dependent part of the heat flux (heat conductivity),

$$\frac{\bar{\mathbf{h}}_\alpha^T}{p_\alpha} = \frac{5}{2} \sum_\beta \widetilde{a}_{\alpha\beta}^{11} n_\beta \widetilde{\nabla T_\beta}, \tag{34}$$

where $\widetilde{a}_{\alpha\beta}^{11}$ is an element from the $\widetilde{A}_{11}$ part of the inverted matrix. In the most common case, where the density of the light species is higher than the density of the heavy species, the impact from cross elements on the light species heat flux is even smaller due to the multiplication with n_β. On the other hand, for the heavy species heat flux, all terms in the sum are comparable; however, it is easy to show that the heavy species heat flux in such a case does not contribute significantly to the global heat balance and therefore the temperature T_0 for light species averaged over all charge states. The temperature of the light species T_0 plays a major role in the thermal force between light and heavy species (see Sec. III B) and thus determines heavy impurity transport.

Thus, in the case with one light and several heavy species, the transport coefficients can be obtained by solving equations for each type of species independently, ignoring cross elements. This allows us to derive analytical expressions for the transport coefficients (see Appendix A).

These expressions are an improved form of the Zhdanov–Yushmanov (ZY) analytical expressions (8.4.7) in Ref. 1. Zhdanov and Yushmanov suggest obtaining transport coefficients keeping only terms with $(m_0/m_i)^0$ order, which directly excludes cross elements from consideration [due to (32)], while the approach discussed in this paper keeps higher order terms $(m_0/m_i)^n$, where $n = 1 \ldots \infty$ in diagonal elements. The reason for this action follows from the fact that the diagonal elements play a major role. Analysis of the matrix in the test cases confirms this fact: even for the mixtures where masses of species become close, cross elements were smaller than diagonal elements. Therefore, higher order terms in diagonal elements affect the answer more than for the cross terms.

To prove this assumption, let us compare the heat conductivity for deuterium in the presence of impurity ions found using this approach with the result using explicit matrix inversion [for solving the algebraic system of equations (8.4.2) in Ref. 1] and the ZY analytical expression (8.4.7) in Ref. 1. Consider the case (deuterium, carbon, and another impurity) where the temperature gradient for both impurities is the same as the temperature gradient for deuterium and the case where the temperature gradient for both impurities is (for some reason) two times higher than for deuterium, to explore what role the difference in ion temperatures plays. In test cases considered in this paper, the amount of carbon and another impurity is chosen according to the rules $\overline{Z_C^2} n_C / n_D = 0.5$, $\overline{Z_I^2} n_I / n_D = 1.0$, where "I" corresponds to another impurity and $\overline{Z_i^2}$ is the averaged square of the impurity charge defined in (A2). The heat flux associated with the deuterium heat conductivity is

$$h_{D\|}^T = -c_D^{(h_T eff)} \frac{n_D T \tau_D^{(Zh)}}{m_D} \nabla_\| T_D, \tag{35}$$

where the transport coefficient $c_D^{(h_T eff)}$ is shown in Fig. 1 and the collision time is defined in Appendix A.

In Fig. 1, different results are plotted: with similar masses and densities for light impurities and small ratios m_D/m_{imp} and n_{imp}/n_D for heavy impurities.

It is clearly shown that $(m_0/m_i)^0$ order accuracy is not sufficient to get good agreement with the explicit matrix inversion result, while the addition of higher order terms only in the diagonal elements provides solutions close to the numerical method except in the hydrogen–helium region, where cross elements in the matrix become important. In this region, a different temperature gradient for the impurity affects the result because both close masses and densities in the impurity term in (34) play a role.

The same comparison can be made for the velocity-dependent part of the heat flux,

$$\bar{h}^w_{\alpha\|} = p_\alpha \sum_\beta c^{(h^A_w)}_{\beta\alpha} (\bar{w}_{\alpha\|} - \bar{w}_{\beta\|}), \tag{36}$$

where the transport coefficient $c^{(h^A_w)}_{\beta\alpha}$ is shown in Fig. 2.

The velocity-dependent part of the deuterium heat flux in the presence of high mass impurities predicted by both original (8.4.7) in Ref. 1 and improved analytical expressions is close to the result obtained from the matrix inversion approach. However, for impurities lighter than beryllium, the improved formula gives a solution much closer to the numerical one (Fig. 2) than the ZY formula. On the other hand, for the high mass species, the calculated heat flux is less accurate (Fig. 2). In the original monograph,[1] it is suggested to set to zero the transport coefficients that represent heavy-light species interactions in the heat flux (velocity-dependent part) for heavy species. Although the improved formula (A28) in Appendix A suppresses the coefficient by a factor $(\mu_{\alpha\beta}/m_\alpha)^{3/2}$ for the cases, where $m_\alpha > m_\beta$, numerical calculation provides an even smaller velocity-dependent part of the heat flux (Fig. 2). In the extreme case, where a difference between masses of species is large, for instance, ion–electron mixture in the simple plasma, the velocity-dependent part is set equal to zero for heavy species.[1,4] Thus, the reduction of the velocity-dependent part for heavy species can be implemented by setting (A28) equal to zero if $m_\alpha/m_\beta < 1$. To keep all expressions the same for both low and high mass species, a smooth analytical approximation to the step function can be applied.

Finally, following Ref. 1, the heat flux for each charge state can be found (see Appendix A).

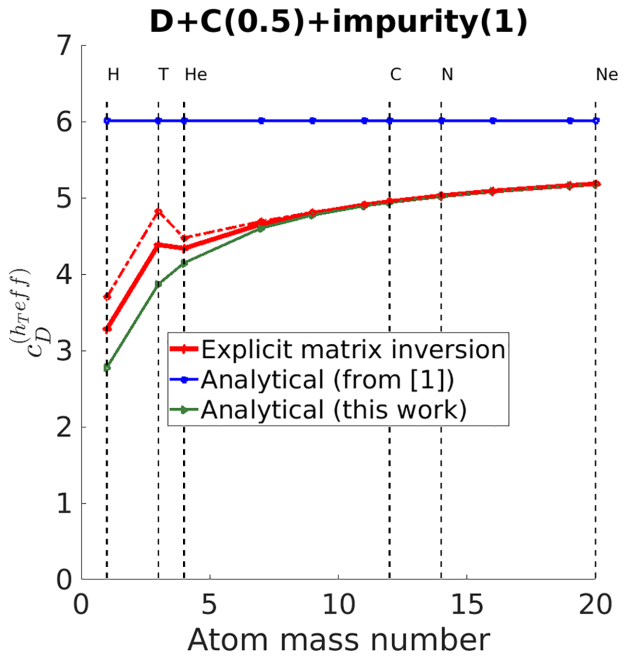

FIG. 1. Temperature-dependent part of the heat flux transport coefficient for deuterium using the explicit solution of the system of equations (8.4.2) in Ref. 1, the original ZY formula (8.4.7) in Ref. 1, and the improved formula (see Appendix A) for the D + C + another impurity case with equal distribution between charge states. The additional impurity is varied along the horizontal axis. The dash-dotted line shows the case where $\nabla_\| T_i = 2 \times \nabla_\| T_D$. The number in parentheses at the top of the figure gives normalized impurity density $[= \overline{Z_i^2} n_i/n_D$ where $\overline{Z_i^2}$ is an averaged square of the charge of impurity, defined in (A2)] and is kept constant.

B. Friction term

Now consider the friction term. According to (8.1.3) in Ref. 1,

$$\mathbf{R}_\alpha \equiv \sum_Z \mathbf{R}_{\alpha Z} = \sum_\beta \left[\bar{G}^{(1)}_{\alpha\beta} (\bar{\mathbf{w}}_\alpha - \bar{\mathbf{w}}_\beta) + \frac{\mu_{\alpha\beta}}{T} \bar{G}^{(2)}_{\alpha\beta} \left(\frac{\bar{\mathbf{h}}_\alpha}{m_\alpha n_\alpha} - \frac{\bar{\mathbf{h}}_\beta}{m_\beta n_\beta} \right) + \left(\frac{\mu_{\alpha\beta}}{T} \right)^2 \bar{G}^{(8)}_{\alpha\beta} \left(\frac{\bar{\mathbf{r}}_\alpha}{m_\alpha n_\alpha} - \frac{\bar{\mathbf{r}}_\beta}{m_\beta n_\beta} \right) \right]. \tag{37}$$

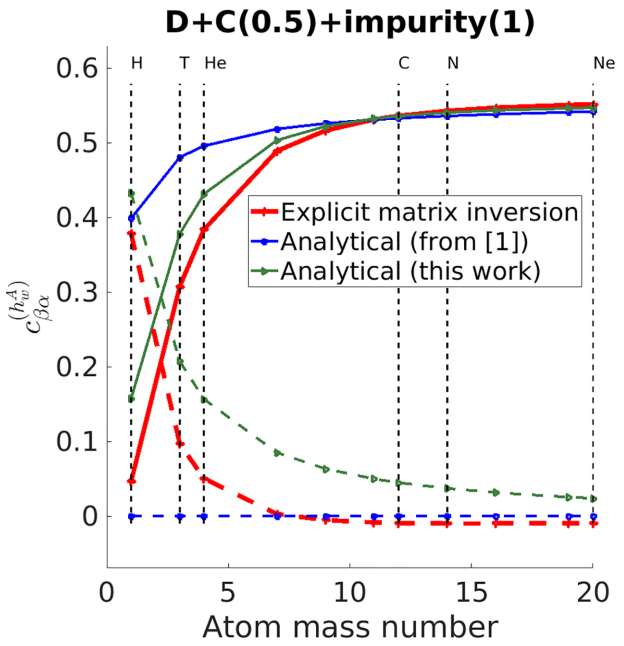

FIG. 2. Velocity-dependent part of the heat flux transport coefficient for the deuterium due to D/impurity velocity difference (solid) and for another impurity due to impurity/D velocity difference (dashed) using explicit solution of the system of equations (8.4.2) in Ref. 1, the original ZY formula (8.4.7) in Ref. 1, and our improved formula (see Appendix A) for D + C + another impurity. (See the caption to Fig. 1 for additional information.)

According to (37), one can conclude that $\sum_\alpha \mathbf{R}_\alpha = 0$ for any velocities, heat fluxes, and r-moments [additional vector moments see Eq. (8.1.2) in Ref. 1] [$\bar{G}^{(1)}_{\alpha\beta}, \bar{G}^{(2)}_{\alpha\beta}, \bar{G}^{(8)}_{\alpha\beta}$ are symmetric regarding to the replacement of $\alpha\beta$ with $\beta\alpha$].

Note that the impact on the friction term of species α from the heat flux and r-moment of species α differs from the impact of the species β terms by factors of m_α/m_β and $(m_\alpha/m_\beta)^2$ correspondingly. Hence, leading terms in both $\mathbf{R}_0$ and $\mathbf{R}_i$, where $i \neq 0$, are dependent on the heat flux and r-moment of the light species and, therefore, on T_0. Thus, where the heat flux/r-moment of heavy species is calculated inaccurately, it does not affect the friction term for heavy species (and light as well) summed over all charge states.

The friction term for each charge state can be found using

$$\mathbf{R}_{\alpha Z} = I_{\alpha Z}\mathbf{R}_\alpha + I_{\alpha Z}\sum_\beta \left[\bar{G}^{(1)}_{\alpha\beta}(\mathbf{w}_{\alpha Z} - \bar{\mathbf{w}}_\alpha) + \frac{\mu_{\alpha\beta}}{m_\alpha}\bar{G}^{(2)}_{\alpha\beta}\left(\frac{\mathbf{h}_{\alpha Z}}{p_{\alpha Z}} - \frac{\bar{\mathbf{h}}_\alpha}{p_\alpha}\right) + \left(\frac{\mu_{\alpha\beta}}{m_\alpha}\right)^2 \frac{m_\alpha}{T}\bar{G}^{(8)}_{\alpha\beta}\left(\frac{\mathbf{r}_{\alpha Z}}{p_{\alpha Z}} - \frac{\bar{\mathbf{r}}_\alpha}{p_\alpha}\right)\right]. \quad (38)$$

Substituting the results of the heat flux and r-moment into (37) and (38), one can obtain analytical transport coefficients for the thermal and friction forces (see Appendix A).

First of all, note that, in the trace-impurity case ($\overline{Z_i^2} n_i / \overline{Z_0^2} n_0 \ll 1$, $m_0 < m_i$), the kinetic numeric factor in Refs. 21 and 22 for the friction force is ≈1 and, for the thermal force, is ≈1.56. However, according to (37), the thermal force depends on the masses of the participants (besides the factor $\sqrt{\mu_{\alpha\beta}}$ in the G-matrices). Indeed, formulas (A53) and (A48) in Appendix A provide kinetic factor ≈1 and $\approx 1.56\,\frac{\mu_{0i}}{m_0}\left[\frac{3}{2} - \frac{1}{2}\frac{\mu_{0i}}{m_0}\right]$ for the friction force and the thermal force correspondingly [here the second term in (A48) for species 0 is absent, which becomes important if $m_0 \approx m_i$]. Thus, the light trace-impurity thermal force in Refs. 21 and 22 is larger than our improved expressions.

Then, consider the thermal force for each type of species summed over all charge states in the non-trace-impurity case for a case (deuterium, carbon, and another impurity) where the temperature gradient for both impurities is the same as the temperature gradient for deuterium and the case where the temperature gradient for both impurities is (for some reason) two times larger than for deuterium, to find where differences in ions temperatures play a role. The transport coefficient for the thermal force averaged over all charge states for carbon and another impurity (Figs. 3 and 4) is described by

$$R^T_\alpha = n_\alpha c_\alpha^{(R^A_T eff)} \nabla_\parallel T_D. \quad (39)$$

Now, we compare these results with the explicit matrix inversion method and the coefficients previously implemented into the SOLPS-ITER code,[21,22] which are based on the ZY analytical expressions (8.4.7) in Ref. 1.

For a deuterium plasma with carbon, the original ZY analytical formula results in a ∼1% deviation from the numerically calculated result. Therefore, for carbon and heavier impurities this formula can be applied, although a slight increase in the deviation for the heavier impurity, due to the presence of carbon, is seen (Fig. 3). Thus, the thermal force averaged over all charge states for nitrogen and neon calculated using the 3.0.6 SOLPS-ITER version and higher (and as a result in Refs. 34–37 and others) is the same as can be obtained by numerically solving the system of equations for heat flux and r-moment (additional vector moment) (8.4.2) in Ref. 1.

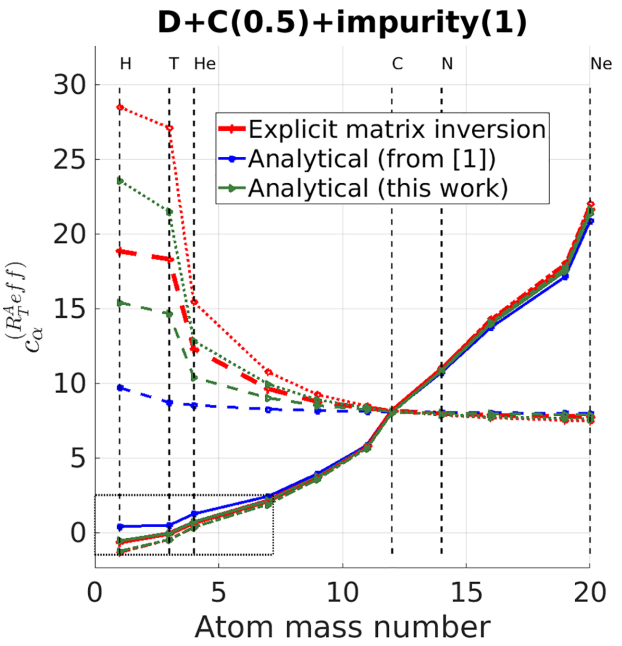

FIG. 3. Temperature-dependent part of the friction term transport coefficient for another impurity (solid) and for carbon (dashed) using explicit solution of the system of equations (8.4.2) in Ref. 1, the original formula from Refs. 21 and 22, and our improved formula (see Appendix A) for D + C + another impurity. Dash-dotted (another impurity) and dotted (carbon) lines are plotted for the case where $\widetilde{\nabla_\parallel T_i} = 2 \times \nabla_\parallel T_D$. (See the caption to Fig. 1 for additional information.)

Furthermore, in the region of heavy impurities, the impurity temperature gradient does not play a role (Fig. 3). Indeed, the shape of the impurity distribution function {represented by impurity heat flux and r-moment [additional vector moment, see Eq. (8.1.2) in Ref. 1] in the Hermite polynomial expansion} is not important in the case where $m_D \ll m_i$, $T_D \approx T_i$ and thus $v_D \gg v_i$. Shaping of the deuterium distribution function driven by $\nabla_\parallel T_D$ is a major effect in such cases.

However, in the light impurity region the situation is different. For cases where $\nabla_\parallel T_D = \widetilde{\nabla_\parallel T_i}$, the analytical ZY expression results in an up to 15% deviation in a (D + C + Li) mixture and up to 90% deviation in a (D + C + He) mixture (Fig. 4). If the temperature of the impurity is different, the deviation is even larger. In contrast, the improved analytical expression for the thermal force in (D + C + Li) gives only a 1% deviation for lithium (Fig. 4) and a 6% deviation for carbon (Fig. 3) from the numerically calculated result. For the (D + C + He) case, the improved formula provides up to 10% deviation for helium (Fig. 4) and up to 16% for carbon (Fig. 3). Note that in this region, the temperature gradient of impurities becomes important.

Notice that deviations for carbon are due to the presence of significant amount of helium ($n_{He}/n_D = 0.4$) and lithium ($n_{Li}/n_D = 0.2$), for smaller amounts of helium/lithium this case is closer to the pure deuterium/carbon. In the ($n_{He}/n_D = 0.04$) case, the deviation from the explicit matrix inversion result is up to 5% for carbon, however, becoming worse for helium: up to 30% (up to 50% for the case, where $\widetilde{\nabla_\parallel T_{He}} = 2 \times \nabla_\parallel T_D$).

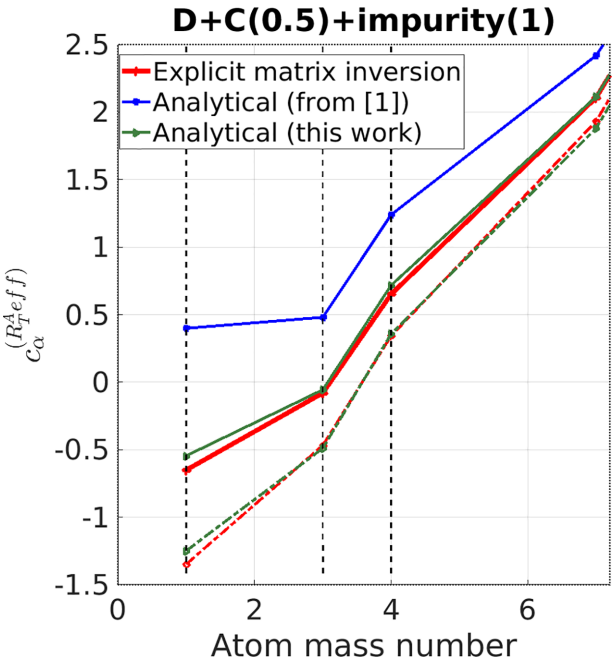

FIG. 4. Zoom of the dotted box in Fig. 3.

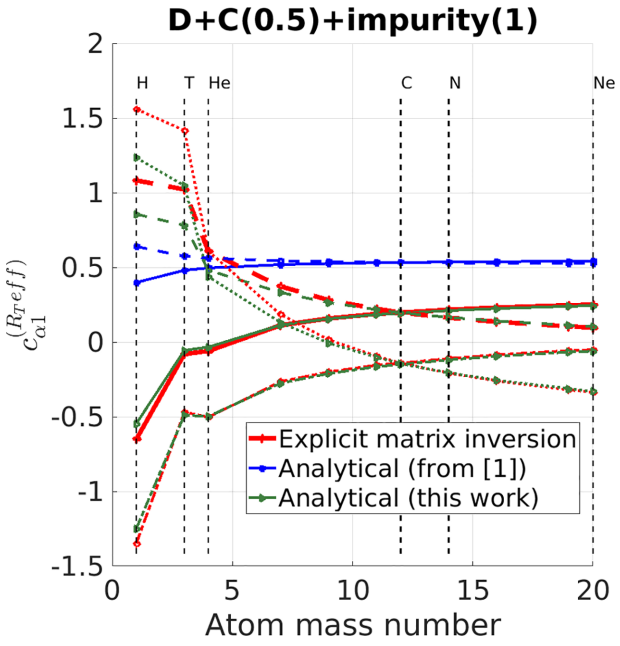

FIG. 5. Temperature-dependent part of the friction term transport coefficient for another impurity $Z = +1$ charge state (solid) and for the carbon $Z = +1$ charge state (dashed) using the explicit solution of the system of equations (8.4.2) in Ref. 1, the original formula from Refs. 21 and 22, and our improved formula (see Appendix A) for D + C + another impurity. Dash-dotted (another impurity $Z = +1$) and dotted (carbon $Z = +1$) lines show the case where $\widetilde{\nabla_\parallel T_i} = \nabla_\parallel T_{i1} = 2 \times \nabla_\parallel T_D$. (See the caption to Fig. 1 for additional information.)

For the cases (deuterium, carbon, and hydrogen) and (deuterium, carbon, and tritium), the original formula (8.4.7) in Ref. 1 provides even the wrong sign (always positive). However, the new formula (A48) in Appendix A works surprisingly well, which confirms the observation made in the tests that even for comparable masses, cross elements play a minor role. In mixtures (D + C+H/T), the thermal force has a deviation for hydrogen/deuterium/tritium of up to 30% (up to 50% for the case, where $\nabla_\parallel T_T = 2 \times \nabla_\parallel T_D$) and for carbon a 15%–20% deviation from the numerically calculated results (Figs. 3 and 4). For more accurate calculations in the case of comparable masses, the explicit solution of the system of equations (8.4.2) in Ref. 1 is required. Moreover, for such cases the temperature gradient of impurities plays a role, and heat fluxes of impurities are important and an accurate calculation of these fluxes is also necessary.

Now, consider the thermal force for each charge state species obtained using (38), which affects space separation between different charge states of the same type of species. Note that this procedure does not require additional assumptions and thus can be made straightforwardly even for mixtures of species with close masses (see Appendix A). What was done for the thermal force in Refs. 21 and 22 represents what is done in the first term in (38); therefore, the dependence on the difference between heat flux and r-moment [additional vector moment, see Eq. (8.1.2) in Ref. 1] averaged over charge states and for each charge state was not taken into account.

Here, again consider the case where the temperature gradient for impurities is the same as the temperature gradient for deuterium, and the case where temperature gradient for impurities (all charge states) is two times larger than for deuterium, to find where the difference in ion temperatures plays a role. In Fig. 5, the transport coefficient for the thermal force for the first charge state for carbon and another impurity described by

$$R_{\alpha 1}^T = n_{\alpha 1} c_{\alpha 1}^{(R_T eff)} \nabla_\parallel T_D \tag{40}$$

is plotted.

According to the thermal force for each charge state, expression (A51) in Appendix A, that is written taking into account the correction to the average thermal force, the first charge state is affected by the correction more than the others, because the impact from the average thermal force is reduced by a factor $1/\overline{Z_\alpha^2}$. It is clearly seen (Fig. 5) that, for the first charge state of the impurity, the correction, represented by the third and fourth terms in (38) (blue curves represent the model from Refs. 21 and 22, plays a role. As a result, the temperature gradient for impurities becomes important (Fig. 5). However, for carbon and higher mass impurities, the thermal force that leads to space separation of each charge state is an order of magnitude smaller than the thermal force that drives impurities, summed over all charge states (Fig. 3). Therefore, it is expected that for the heavy impurities, their temperature gradient affects slightly the charge states space distribution, but not the global impurity transport.

Then, consider the friction force for each type of species summed over all charge states. Take a look at the case (deuterium, carbon and another impurity). In Fig. 6 are plotted transport coefficients for the friction force, averaged over all charge states, for carbon and another impurity, described by

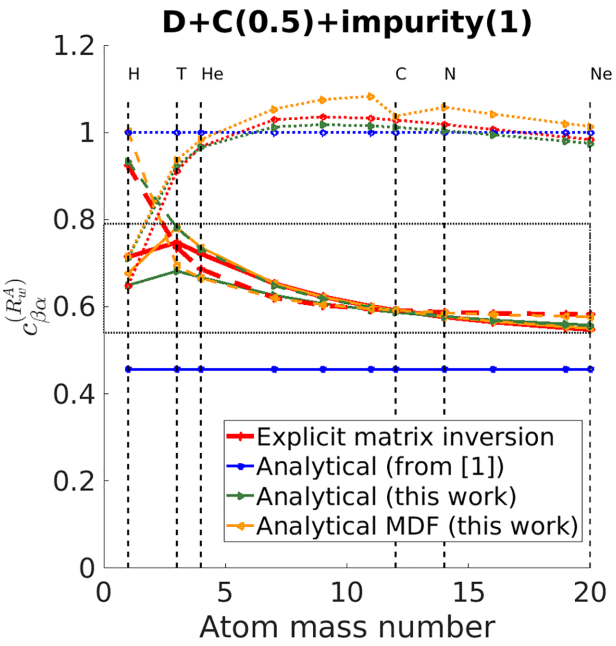

FIG. 6. Velocity-dependent part of the friction term transport coefficient for another impurity/deuterium (solid), for carbon/deuterium (dashed), and for another impurity/carbon (dotted) using the explicit solution of the system of equations (8.4.2) in Ref. 1, the original formula from Refs. 21 and 22, and our improved formula (see Appendix A) for the D + C + another impurity case. (See the caption to Fig. 1 for additional information.)

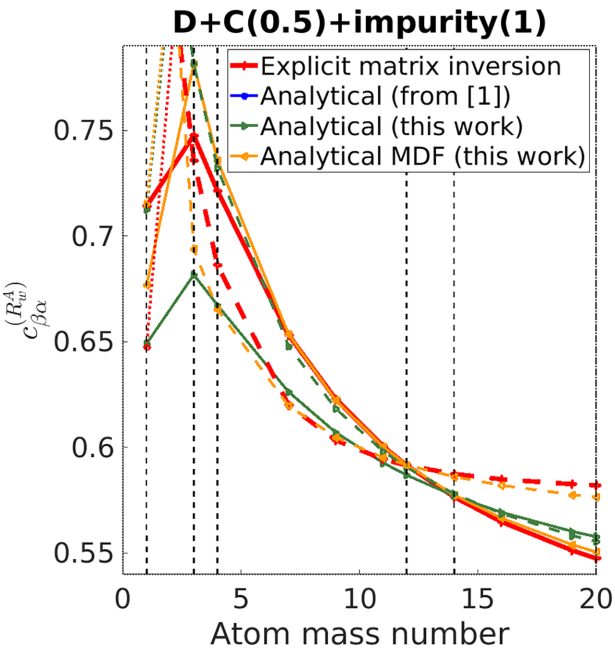

FIG. 7. Zoom of the dotted box in Fig. 6.

$$R_\alpha^{\mathbf{w}} = -n_\alpha \sum_\beta \frac{\mu_{\alpha\beta}}{\tau_{\alpha\beta}^{(Zh)}} c_{\beta\alpha}^{(R_w^A)} (\bar{w}_{\alpha\|} - \bar{w}_{\beta\|}), \tag{41}$$

where definitions can be found in Appendix A.

The transport coefficient for the friction force between deuterium and impurity predicted by the original ZY analytical expression (8.4.2) in Ref. 1, that is used in Refs. 21 and 22 is underestimated significantly for all realistic cases compared to the direct numerical solution of the system of equations (8.4.2) in Ref. 1 (Fig. 6): 37% for helium, 23% for carbon, 17% for neon. This difference in the friction force can affect impurity transport.[38] On the other hand, our improved expression is much closer to the numerical solution (for a discussion of the corresponding deviations see below). This is the result of the inclusion of next order terms in the mass ratio m_0/m_i. Indeed, one can see (see Appendix A) that, under the assumption $m_0/m_i = 0$, our improved expression turns into the original ZY formula (8.4.2) in Ref. 1.

Moreover, as it was discussed in the Sec. III A (Fig. 2), for the heavy species, the velocity-dependent part of the heat flux is not calculated precisely by our improved expression. The same result can be obtained for the velocity-dependent part of the r-moment [additional vector moment, see Eq. (8.1.2) in Ref. 1]. This inaccuracy for the heat flux and r-moment affects the friction force. Therefore, it is necessary to suppress them to zero to get a better match with the numerical result. One way to do this is by setting coefficients (A28) and (A39) equal to zero, if $m_\alpha/m_\beta < 1$. The result, an even better match [indicated as "Analytical MDF (this work)" in Figs. 6 and 7, while "Analytical (this work)" corresponds to unmodified heat flux and r-moment] with the numerical result, with the deviation from the matrix inversion solution: for tritium 5% vs 8%, for helium 2% vs 8%, for carbon 0.03% vs 0.7%, and for neon 0.6% vs 2% (for carbon in the presence of neon 1% vs 5%). However, the mismatch for another impurity/carbon friction force becomes worse (Fig. 6). Note that the transport coefficient, equal to unity for impurity/impurity interaction (used in Refs. 21 and 22, is close to the explicit approach result for most cases. Besides, a correction for the friction force between different charge states can be applied (see Appendix A), though for heavy species this transport coefficient is ≈ 0.8–1.0 and significantly differs from unity only for light species.

C. Viscous stress tensors

Finally, using a similar approach for the viscous stress tensors equations (26) and (27), one can obtain analytical expressions for both the velocity and heat flux-dependent parts of the viscous stress tensors (see Appendix A). Now again consider the deuterium, carbon, and another impurity case. The viscous stress tensor for species α summed over all charge states (for comparison with the analytical result from the matrix inversion method, we assume $W_{|||}^{\bar{h}_\beta}/n_\beta = W_{|||}^{\bar{h}_\alpha}/n_\alpha$ for arbitrary β)

$$\bar{\pi}_{\alpha|||} = -p_\alpha \tau_\alpha^{(Zh)} c_\alpha^{(\pi_u^A eff)} W_{||||} - \tau_\alpha^{(Zh)} c_\alpha^{(\pi_h^A eff)} W_{|||}^{\bar{h}_\alpha}. \tag{42}$$

In Figs. 8 and 9, $c_\alpha^{(\pi_u^A eff)}$, $c_\alpha^{(\pi_h^A eff)}$ are plotted. Other definitions can be found in Appendix A.

It is shown (Fig. 8) that, for light species, the original ZY expression overestimates the explicit method result significantly, while the new formula provides a closer result. Close answers are obtained for the heat flux-dependent part of the viscous stress tensor using both the

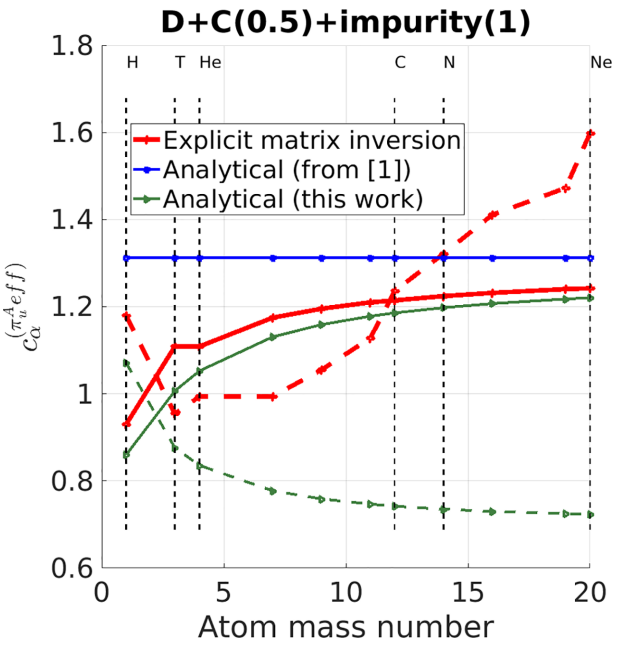

FIG. 8. Velocity-dependent part of the viscosity transport coefficient for the deuterium (solid) and for another impurity (dashed) using the explicit solution of the system of equations (26) and (27), the original ZY formula,[1] and our improved formula (see Appendix A) for the D + C + another impurity case. (See the caption to Fig. 1 for additional information.)

improved formula and matrix inversion calculation (Fig. 9). For this part, the analytical expression in Ref. 1 was not presented. For the case $m_D/m_{imp} \approx 1$ and $n_{imp}/n_D \approx 1$, the analytical method works quite well (Figs. 8 and 9). However, for the heavy impurities, the analytical expression does not match the calculated answer, and this affects the impurity momentum equation. On the other hand, the total momentum equation (summed over all species) is mainly affected by the light component viscous stress tensor (in case $m_D/m_{imp} < 1$ and $n_{imp}/n_D < 1$), and $\mu_{\alpha 1}, \mu_{\alpha 2}$ as discussed in Ref. 14 can be obtained in the Pfirsch–Schlüter regime in the presence of impurities using expressions from Appendix A.

D. Summary

New analytical expressions discussed in this section and presented in Appendix A can be applied for the cases with one light and several heavy ions, when heat flux and viscous stress tensor of the heavy species does not affect the solution (for example, $n_{imp}/n_D < 1$). For plasmas where the mass of the main component is not significantly different from the mass of the impurity, improved expansions provide solutions closer to the numerical one than can be obtained by the original expression in Ref. 1. Moreover, for impurities lighter than the main ions, the sign of the new thermal force is inverted; therefore, our new expressions provide a qualitatively correct result. Furthermore, new expressions are written in general form without specifying which species are main ions or impurities, and which species are light or heavy, as it was for the original analytical expressions in Refs. 1, 21, and 22 Besides, these formulas describe transport for each charge state of all the ions. Therefore, it allows us to consider helium plasmas with impurities, which was not possible in the previous SOLPS-ITER model, where main ions were assumed to be singly ionized. However, either of the purpose of accurate transport calculations for mixtures with close masses or where high order moments of the heavy species distribution function heat flux, r-moment [additional vector moment, see Eq. (8.1.2) in Ref. 1], viscous stress tensor, σ-moment [additional tensor moment see Eq. (8.1.2) in Ref. 1] are important, the explicit approach discussed in Sec. II should be applied. Finally, it is important to mention that these results can be applied only for collisional plasmas, since time derivatives and gradients [which are of the order of $(\lambda/L)^2$, where λ is a mean free path and L is a space scale of the gradients] were neglected in high order moments equations (heat flux, r-moment, viscous stress tensor, σ-moment).[1] Sometimes, the heat flux-dependent part of the stress-viscous tensor can be of the same order as the velocity contribution. Therefore, the heat flux contribution is added to the viscous stress tensor and σ-moment equations (26) and (27) for taking into account the Pfirsch–Schlüter regime effects discussed in Refs. 14, 15, and 27 In the case of less collisional plasmas, next order terms have to be considered as well.

IV. APPLICATION OF GRAD'S CLOSURE TO SOLPS-ITER

A. Heat flux, friction, and heat exchange terms

First of all, it is important to mention that, in the current SOLPS-ITER model, ion temperatures $T_{ions}^{(Br)}$ are considered to be equal for all ions;[17] therefore, (3) has to be summed over all ions. It should be noted that even in this case, $T_{\alpha Z}$ can be different due to (15). Second, the part of the heat flux that depends on the velocity difference between ions with different masses [last term in (23)] is not present in models which are based on the Braginskii equations (where such a term appears only in the electron heat flux) and has been neglected in multicomponent cases;[19,39–42] in future this contribution should be added. Moreover, the effective ion conductivity also changes in plasmas with non-trace-impurities, even under the assumption of identical temperature for all ions. In Fig. 10, it is shown how the ion heat conductivity calculated using the explicit matrix inversion approach is different from what is predicted by the current SOLPS-ITER model (Sec. B.4 in Ref. 26.

A comparison of the friction and thermal force between the current SOLPS-ITER model Refs. 21 and 22, our improved expressions, and the explicit approach is made in detail in Sec. III B. Therefore, it is not repeated here. The improved formulas for the friction and thermal forces have been implemented into the SOLPS-ITER code. Test results can be found in Sec. IV C.

In the current SOLPS-ITER model (Secs. C.3.1 and C.4.1 in Ref. 26), the heat source, due to the friction between different ions and with electrons, in heat exchange terms for ions $Q_{ions}^{(Br)}$ and electrons $Q_e^{(Br)}$ is written so as to ensure the global conservative property in collisions.[4] Using (18) for electrons and ions, the distribution between electron and ion channels can be found more accurately. One can use (18) to find the correct heat distribution between different ions, as well.

B. Viscous stress tensor

Consider an orthogonal curvilinear coordinate system where x is a poloidal coordinate and y is a radial coordinate (43), as it is done in Ref. 16,

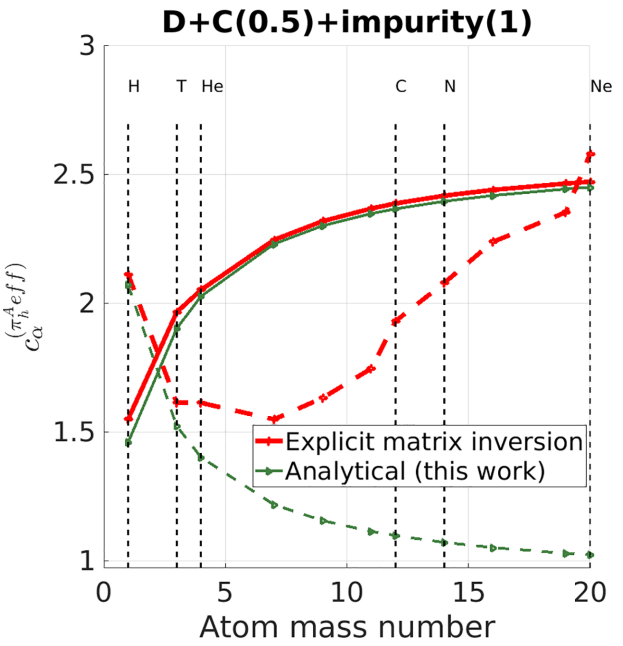

FIG. 9. Heat flux-dependent part of the viscosity transport coefficient for the deuterium (solid) and for another impurity (dashed) using the explicit solution of the system of equations (26) and (27) and our improved formula (see Appendix A) for the D + C + another impurity case. (See the caption to Fig. 1 for additional information.)

$$b_x = \frac{B_x}{B},\ h_x = \frac{1}{||\nabla x||},\ h_y = \frac{1}{||\nabla y||},\\ h_z = \frac{1}{||\nabla z||},\ \sqrt{g} = h_x h_y h_z. \tag{43}$$

In this coordinate system (43) and under the assumption that $n_{\alpha Z}, T_{\alpha Z}, \varphi$ are flux surface functions inside the separatrix where parallel viscosity plays its larger role[14,15] in the parallel momentum balance, Eq. (B7) in Appendix B turns into

$$\left(\nabla\cdot\overleftrightarrow{\pi}_{\alpha Z}^{(par)}\right)_{||} = -\frac{4}{3}b_x B^{3/2}\frac{\partial}{h_x\partial x}\left[\frac{b_x}{B^2}\frac{n_{\alpha Z}}{n_\alpha}\left[\sum_\beta \tilde{c}_{\alpha\beta}^{(\pi_u^A)}\tau_{\beta\alpha}^{(Zh)}p_\beta\frac{\partial}{h_x\partial x}\right.\right.\\ \left.\times\left(\frac{\sqrt{B}}{b_x}u_x\right) + 2c_\alpha^{(\pi_u^B)}\tau_{\alpha\alpha}^{(Zh)}\frac{\overline{Z_\alpha^2}}{Z^2}p_\alpha\frac{\partial}{h_x\partial x}\left(\frac{\sqrt{B}}{b_x}u_x\right)\right]\\ -\frac{8}{15}b_x B^{3/2}\frac{\partial}{h_x\partial x}\left[\frac{b_x}{B^2}\frac{n_{\alpha Z}}{n_\alpha}\left[\sum_\beta\left(\tilde{c}_{\alpha\beta}^{(\pi_h^A)}\tau_{\beta\alpha}^{(Zh)}\frac{\partial}{h_x\partial x}\right.\right.\right.\\ \left.\times\left(\frac{\sqrt{B}}{b_x}\bar{h}_{\beta x}\right)\right) + 2c_\alpha^{(\pi_h^B)}\tau_{\alpha\alpha}^{(Zh)}\frac{\overline{Z_\alpha^2}n_\alpha}{Z^2 n_{\alpha Z}}\\ \left.\left.\times\frac{\partial}{h_x\partial x}\left(\frac{\sqrt{B}}{b_x}h_{\alpha Zx}\right)\right]\right]. \tag{44}$$

Note that expression (44) is a generalization of the corresponding terms in the momentum equation in Refs. 16 and 17 for the multicomponent case. The present SOLPS-ITER model for the stress-viscosity tensor can be insufficiently accurate for the multiple ions case in the high collisionality limit. The new result is compared with that currently applied for SOLPS-ITER in the Pfirsch–Schlüter regime[17] in Fig. 10. Despite the fact that the effect on the viscous stress tensor (velocity part) π_{ion}^u summed over all ions is not more than 8% due to the new approach, the effect on the impurity viscous stress tensor (velocity part) is significant. For high mass high-Z impurity (carbon and higher), the viscous stress tensor (velocity part) is ≈ 1.5–2.5 times higher than currently implemented in SOLPS-ITER. This is the result of two effects: (1) the ratio $\sqrt{2\mu_{\alpha\beta}/m_\alpha}$, which differs from unity for heavy impurities, should be added into the definition of the collision time used by SOLPS-ITER and (2) transport coefficients should be calculated accurately using this approach. The heat flux-dependent part of the viscous stress tensor π_{ion}^h (whose importance was discussed above) can be 20% higher for this closure (assuming for comparison $W_{||||}^{\bar{h}_\beta}/n_\beta = W_{||||}^{\bar{h}_{ion}}/n$ for either β) than for the current SOLPS-ITER approach (Fig. 10). The impurity viscous stress tensor (heat flux-dependent part) is currently not included.

C. Test cases using improved expressions

In Fig. 6, one can see that, even for deuterium plasmas with neon non-trace-impurity transport coefficient, the friction force calculated by the original ZY formula Eq. (8.4.2) in Ref. 1 is different compared to our improved treatment, while the thermal force remains the same (Fig. 3). That should affect neon transport in the tokamak. For the range of parameters applicable ITER baseline scenarios, the parallel neon transport is determined by the balance of the thermal and friction forces due to the interaction with deuterium.[34] Thus, the new friction and thermal force treatments were implemented into the SOLPS-ITER code and tested for a deuterium and neon ITER case. However, the improved ion thermal conductivity and stress-viscosity tensor formulations have not been included yet. We present two cases, a reference case, run with the original model for the friction and thermal force terms, and a simulation where our new treatment is applied. These cases are catalogued in the ITER integrated modeling analysis suite (IMAS) database as 123081 and 123082, respectively. For the test, an intermediate case between cases 1b (123014) and 2b (123018) (with drifts) was chosen from those that are discussed in Ref. 34, with parameters: divertor neutral pressure p_n = 7.5 Pa and relative Ne concentration, separatrix-averaged, $c_{Ne} = 1.0\%$. To illustrate the changes in the impurity transport due to the new thermal and friction force treatments, the neon density is plotted in Fig. 11.

One can see that, even for the deuterium and neon plasma, the mass difference is not high enough to assume $m_D/m_{Ne} \approx 0$. The application of the new formulas can observably affect the impurity transport for such cases. Also, after implementation of the new expressions, the relative separatrix-averaged Ne concentration dropped to $c_{Ne} = 0.8\%$, while the neon seeding rate is kept constant (6.0×10^{19} particles/s). In these tests, neon throughput (in the steady-state) and pumping speed below the divertor dome are kept constant. However, actual extraction of neon from the divertor by the pumping system, which depends on the distribution between neon flows in the divertor (part goes into the pumping system and part goes upstream), slightly increases, which was seen on the run diagnostics during the simulation. This leads to 10% drop of the amount of neon in the whole computational domain and in the core, in particular. It is interesting to note that the amount of neon in the outer divertor

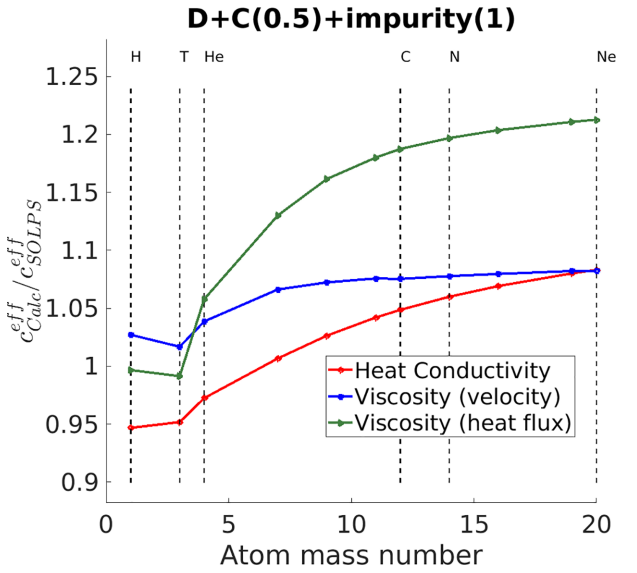

FIG. 10. Ratio of the effective transport coefficient calculated using the explicit solution of the system of equations (8.4.2) in Ref. 1, (26), and (27) to the current SOLPS-ITER model[26] for the D + C + another impurity. Here $h^T_{ions\|Calc/SOLPS} = -c^{eff}_{Calc/SOLPS}\nabla_\| T^{(Br)}_{ions}$; $\pi^u_{ions\|\|Calc/SOLPS} = -c^{eff}_{Calc/SOLPS}W_{\|\|}$; $\pi^h_{ions\|\|Calc/SOLPS} = -c^{eff}_{Calc/SOLPS}W^{h_{ions}}_{\|\|}$ [W-tensors see Eq. (A9) of Appendix A], where $c^{eff}_{Calc/SOLPS}$ coefficients are chosen using either current SOLPS-ITER expressions or explicit approach of solving system algebraic equations of high order moments (8.4.2) in Ref. 1, (26), and (27). (See the caption to Fig. 1 for additional information.)

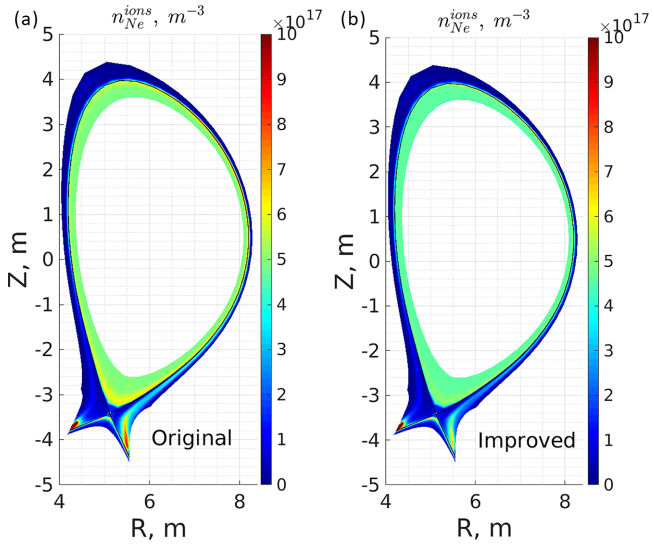

FIG. 11. 2D neon density distribution (summed over all ions) for the two identical ITER modeling cases using the SOLPS-ITER code, in which the original expressions from Refs. 21 and 22 are applied (123081) (a) and our improved expressions are applied (123082) (b).

region decreases by 20%, while the amount of neon in the inner divertor region does not change significantly. As a result, the peak power loading of the outer divertor target increases by ≈1 MW/m^2 (Fig. 12). This impact on the neon distribution should be investigated further.

It is also interesting to note that in the regions with low amounts of neon, the thermal force coefficients are slightly smaller, while the friction force remains the same according to the kinetic coefficients for the trace-impurity regime, which is different to the non-trace-impurity regions, where transport coefficients follow behaviors described in Figs. 3 and 7. This example again shows that an accurate treatment of the main component distribution function shape affects the impurity transport both for the trace-impurity and non-trace-impurity cases. We use these demonstration runs to illustrate that our improved expressions for the transport coefficients affect impurity transport in tokamaks like ITER. Further detailed analysis is required to understand this impurity behavior and its consequences on machine operation more fully. Detailed analysis is now under way to understand this impurity behavior.

It is necessary to mention that, for this test, the expressions for thermal (A51) and friction forces (A60) in Appendix A were slightly reduced. The thermal force for the impurity type I and charge state "Z" is assumed to be

$$R^T_{IZ} = c^{(R^A_T)}_{0I}\frac{Z^2 n_{IZ}}{Z^2_0}\nabla T^{(Br)}_{ions}. \quad (45)$$

The friction force for the impurity type I and charge state Z is assumed as

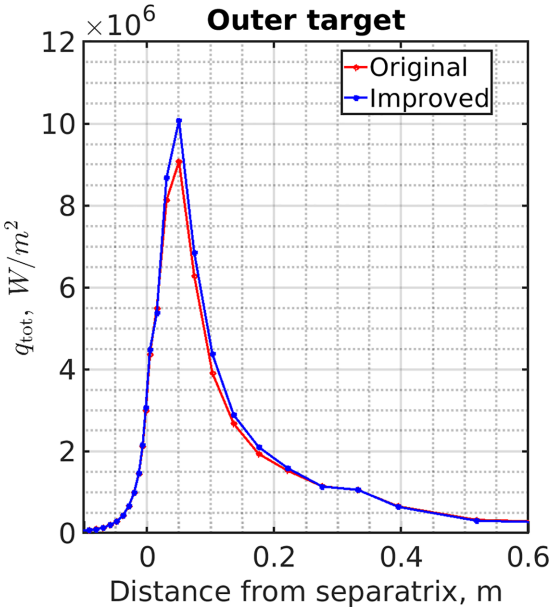

FIG. 12. The outer target total power load, which includes ions/electrons energy flux (major contribution), ion recombination loads, recycled neutrals energy flux (returns part of the incoming energy back to the plasma volume), radiation loads, and other neutral/surface interaction, for the two identical ITER modeling cases using the SOLPS-ITER code, in which the original expressions from Refs. 21 and 22 are applied (123081) and our improved expressions are applied (123082).

$$R_{IZ}^{\mathbf{w}} = -n_I I_{IZ} \frac{\mu_{I0}}{\tau_{I0}^{(Zh)}}(1 + c_{I0}^{(R_w^A 1)})(\mathbf{w}_{IZ} - \mathbf{w}_0) - n_I I_{IZ} \sum_{\beta \neq 0} \frac{\mu_{I\beta}}{\tau_{I\beta}^{(Zh)}}(\mathbf{w}_{IZ} - \bar{\mathbf{w}}_\beta), \quad (46)$$

where "0" is connected to the main light single charge state ion, and thermal and friction forces for the main ions are

$$R_0^T = -\sum_{\beta \neq 0} n_0 c_{0\beta}^{(R_T^A)} \frac{\overline{Z_\beta^2} n_\beta}{\overline{Z_0^2} n_0} \nabla T_{ions}^{(Br)}, \quad (47)$$

$$R_0^{\mathbf{w}} = -n_0 \sum_{\beta \neq 0} \frac{\mu_{0\beta}}{\tau_{0\beta}^{(Zh)}}(1 + c_{I0}^{(R_w^A 1)})(\mathbf{w}_0 - \bar{\mathbf{w}}_\beta). \quad (48)$$

On the one hand, such an approach allows us to change only transport coefficients for this first test without rewriting equations significantly. On the other hand, for the deuterium and neon case these expressions provide close results to (A51) and (A60) in Appendix A. However, full (A51) and (A60) will be implemented into the SOLPS-ITER code later without specifying main ions and impurities explicitly.

Finally, let us discuss the applicability of this method for ITER modeling. Thus, we compare the effective free path of the deuterium $[\lambda_D^{eff} = \sqrt{2T_{ions}/m_D} \cdot \tau_D^{(Zh)}]$ with the length scale of the ion temperature gradient along the magnetic field $(T_{ions}^{loc\,max} - T_{ions}^{loc\,min})/|\nabla_\parallel T_{ions}|$ (Fig. 13), where $T_{ions}^{loc\,max}$, $T_{ions}^{loc\,min}$ are the local extrema along the magnetic field, for example, on the closed magnetic surfaces the local maximum is at the bottom and the local minimum is at the top of the tokamak due to the ion gradient B drift, and in the near-SOL, the local maximum is at the upstream point and the local minimum is at the targets. For neon, the Knudsen number is of the same order or smaller. One can see that, in the SOL, the Knudsen number is $Kn \approx 10^{-2} - 10^{-1}$; therefore, the calculation of the thermal force and ion heat conductivity using this method can be applied. The friction force is usually balancing the thermal force, and, as a result the flow velocity difference, which is driven by the temperature gradient, is lower than the ion sound speed. However, in the confinement region, the Knudsen number is $Kn > 1$, and this method is not accurate enough. Thus, an extension into the collisionless range using neoclassical results is required.

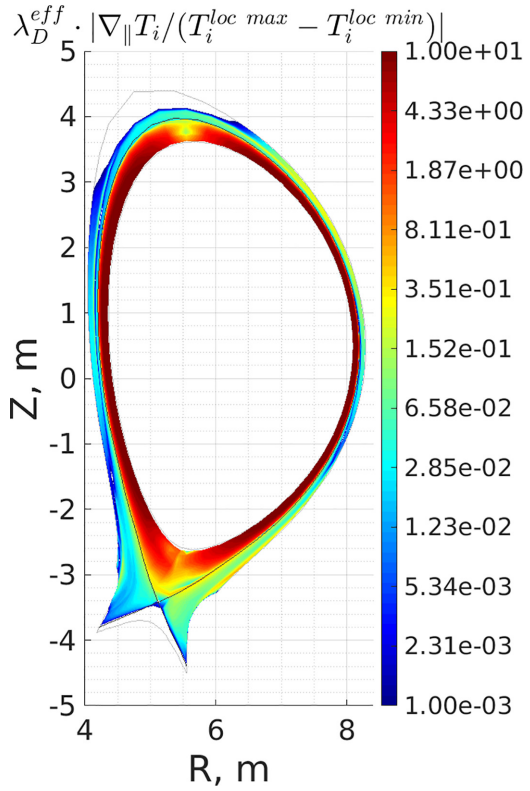

FIG. 13. The Knudsen number according to the ion temperature gradient scale $Kn = \lambda_D^{eff} \cdot |\nabla_\parallel T_{ions}/(T_{ions}^{loc\,max} - T_{ions}^{loc\,min})|$, where λ_D^{eff} is the deuterium effective mean free path and $T_{ions}^{loc\,max}$, $T_{ions}^{loc\,min}$ are the local extrema along the magnetic field. The color bar is on a logarithmic scale and the white region is below the scale.

V. CONCLUSIONS

This paper tackles the closure in the parallel direction of the system of fluid equations using Grad's moment method[5] for multicomponent collisional plasmas and extends the study made in Refs. 1 and 6. The method allows one to obtain transport coefficients for the heat flux, friction, and viscosity terms for each charge state of each species for arbitrary plasma compositions, including deuterium + tritium + helium + other impurities mixtures, where densities and masses of species can be comparable. Therefore, this approach can be implemented into SOLPS-ITER[19,20] or other fluid codes to model this mixture for future reactors (ITER,[31] DEMO,[32] CFETR[33] and complex compositions in existing machines.

In contrast to previous papers devoted to such an approach,[7,12] two major improvements are made: corrections for the direct implementation of the closure Ref. 1 into the Braginskii equations and the heat flux-dependent part of viscous stress tensor. The importance of this part was discussed in Refs. 14 and 15. In this paper, the result in collisional regime is extended to arbitrary plasma mixtures.

New analytical expressions were developed (see Appendix A), which provide a better match to the explicit matrix inversion method for the heat flux, friction, and viscosity term and extend the applicability of the analytical approach to lower mass impurities. Moreover, this accurate treatment for multicharge state ions allows for the use of our analytical approach for cases where all ions have multiple charge states, for example, helium plasmas with impurities, which was not possible with the original expressions.

These new friction and thermal force terms descriptions have been implemented into the SOLPS-ITER code and tested for an ITER deuterium plasma with non-trace-impurity neon and compared with the current SOLPS-ITER model.[21,22] Even for such a mixture, the new formulas show different impurity transport behavior confirming that the $m_D/m_{Ne} \ll 1$ assumption is not accurate enough. Thus, further studies of the impurity transport in ITER and other devices using this improved approach are required.

ACKNOWLEDGMENTS

This work has been carried out within the framework of the EUROfusion Consortium and has received funding from the Euratom research and training programme 2014-2018 and 2019-2020 under grant agreement No 633053. This work was performed in part under the auspices of the ITER Scientist Fellow Network. The views and opinions expressed herein do not necessarily reflect

those of the European Commission or of the ITER Organization. The work of V. A. Rozhansky, E. G. Kaveeva, and I. Y. Senichenkov was supported by task "Razrabotka teoreticheskih modelej i integrirovannyh kodov novogo pokoleniya dlya adekvatnogo opisaniya stacionarnoj termoyadernoj plazmy v energeticheskom reaktore na osnove tokamaka."

APPENDIX A: DETAILED FORMULAS FOR THE IMPROVED ANALYTIC MODEL

In this appendix, we provide the improved analytical expressions for the kinetic coefficients along the magnetic field in the collisional multicomponent plasma.

1. Definitions

Here are defined the variables used in this paper:
Reduced mass

$$\mu_{\alpha\beta} = \frac{m_\alpha m_\beta}{m_\alpha + m_\beta}. \tag{A1}$$

Variables averaged over charge states

$$\overline{Z_\alpha^2} n_\alpha = \sum_Z Z^2 n_{\alpha Z}, \quad I_{\alpha Z} = \frac{Z^2 n_{\alpha Z}}{\overline{Z_\alpha^2} n_\alpha}, \tag{A2}$$

$$\bar{\mathbf{w}}_\alpha = \sum_Z I_{\alpha Z} \mathbf{w}_{\alpha Z}, \quad \bar{\mathbf{h}}_\alpha = \sum_Z \frac{p_\alpha I_{\alpha Z} \mathbf{h}_{\alpha Z}}{p_{\alpha Z}}, \tag{A3}$$

$$\bar{\mathbf{r}}_\alpha = \sum_Z \frac{p_\alpha I_{\alpha Z} \mathbf{r}_{\alpha Z}}{p_{\alpha Z}}, \quad \bar{\pi}_{\alpha|||} = \sum_Z \frac{p_\alpha I_{\alpha Z} \pi_{\alpha Z|||}}{p_{\alpha Z}}. \tag{A4}$$

Definitions connected to the moments of the distribution function

$$\mathbf{w}_{\alpha Z} = \mathbf{u}_{\alpha Z} - \mathbf{u}, \quad \mathbf{u} = \frac{\sum_{\alpha,Z} m_\alpha n_{\alpha Z} \mathbf{u}_{\alpha Z}}{\sum_{\alpha,Z} m_\alpha n_{\alpha Z}}, \tag{A5}$$

$$n = \sum_\alpha n_\alpha, \quad n_\alpha = \sum_Z n_{\alpha Z}, \quad p_{\alpha Z} = n_{\alpha Z} T_{\alpha Z}, \tag{A6}$$

$$nT = \sum_\alpha n_\alpha T_\alpha, \quad p_\alpha = n_\alpha T_\alpha = \sum_Z n_{\alpha Z} T_{\alpha Z}, \tag{A7}$$

$$n_\alpha \widetilde{\nabla T_\alpha} = \sum_Z n_{\alpha Z} \nabla T_{\alpha Z}. \tag{A8}$$

Higher order moments are defined in the main text (11)–(13). $\mathbf{r}_{\alpha Z}$ (additional vector moment) and $\vec{\sigma}_{\alpha Z}$ (additional tensor moment) are defined in Ref. 1 Eq. (8.1.2).

W-tensors in arbitrary Cartesian coordinate system are

$$\begin{gathered} W_{|||} = B_k B_l W_{kl}/B^2, \\ W_{kl} = 2\left[\frac{1}{2}\left(\frac{\partial u_k}{\partial x_l} + \frac{\partial u_l}{\partial x_k}\right) - \frac{1}{3}\delta_{kl}\nabla\cdot\mathbf{u}\right], \\ W_{|||}^{\bar{h}_\alpha} = B_k B_l W_{kl}^{\bar{h}_\alpha}/B^2, \end{gathered} \tag{A9}$$

$$W_{kl}^{\bar{h}_\alpha} = \frac{4}{5}\left[\frac{1}{2}\left(\frac{\partial \bar{h}_{\alpha k}}{\partial x_l} + \frac{\partial \bar{h}_{\alpha l}}{\partial x_k}\right) - \frac{1}{3}\delta_{kl}\nabla\cdot\bar{\mathbf{h}}_\alpha\right], \tag{A10}$$

where parallel velocity and drift contributions—diamagnetic and E × B drift velocities—should be taken into account in (A9). Heat flux in (A10) should contain the parallel contribution determined in this paper and the diamagnetic contribution (see Appendix B).

Collisional right-hand sides of Eqs. (8.1.6) and (8.1.6') in Ref. 1 are defined as

$$R_{\alpha Z rs}^{20} = m_\alpha \int\int\int \left(c_k c_l - \frac{\delta_{kl}}{3}\mathbf{c}^2\right) C_{\alpha Z} d^3\mathbf{v}, \tag{A11}$$

$$R_{\alpha Z rs}^{21} = \frac{m_\alpha}{2} \int\int\int \left(\mathbf{c}^2 - 7\frac{T_{\alpha Z}}{m_\alpha}\right)\left(c_k c_l - \frac{\delta_{kl}}{3}\mathbf{c}^2\right) C_{\alpha Z} d^3\mathbf{v}, \tag{A12}$$

where $\mathbf{c} = \mathbf{v} - \mathbf{u}$. Therefore, after the distribution function substitution and linearization Ref. 1, parallel–parallel components of the summed over charge states right-hand sides $\bar{R}_{\alpha|||}^{2*}$ are

$$\bar{R}_{\alpha|||}^{20} = \sum_\beta \frac{T}{m_\alpha + m_\beta}\left[\frac{\bar{G}_{\alpha\beta}^{(3)}\bar{\pi}_{\alpha|||}}{p_\alpha} + \frac{\bar{G}_{\alpha\beta}^{(4)}\bar{\pi}_{\beta|||}}{p_\beta} + \frac{\mu_{\alpha\beta}}{T}\left(\frac{\bar{G}_{\alpha\beta}^{(13)}\bar{\sigma}_{\alpha|||}}{p_\alpha} + \frac{\bar{G}_{\alpha\beta}^{(14)}\bar{\sigma}_{\beta|||}}{p_\beta}\right)\right], \tag{A13}$$

$$\bar{R}_{\alpha|||}^{21} = \sum_\beta \frac{T}{m_\alpha + m_\beta}\left[\frac{7}{2}T\mu_{\alpha\beta}\left(\frac{\bar{G}_{\alpha\beta}^{(13)}\bar{\pi}_{\alpha|||}}{m_\alpha^2 p_\alpha} + \frac{\bar{G}_{\alpha\beta}^{(14)}\bar{\pi}_{\beta|||}}{m_\beta^2 p_\beta}\right) + \frac{\bar{G}_{\alpha\beta}^{(15)}\bar{\sigma}_{\alpha|||}}{p_\alpha} + \frac{\bar{G}_{\alpha\beta}^{(16)}\bar{\sigma}_{\beta|||}}{p_\beta}\right]. \tag{A14}$$

For the G-matrices definitions, see in Ref. 1 and corrections in Appendix C.

Collision times are defined by

$$\lambda_{\alpha\beta} = \frac{1}{3}(2\pi)^{-3/2}\overline{Z_\alpha^2} n_\alpha \overline{Z_\beta^2} n_\beta \sqrt{\mu_{\alpha\beta}} \frac{\ln\Lambda}{T^{3/2}}\left(\frac{e^2}{\varepsilon_0}\right)^2, \tag{A15}$$

$$\tau_{\alpha\beta}^{(Zh)} = \frac{n_\alpha \mu_{\alpha\beta}}{\lambda_{\alpha\beta}}, \tag{A16}$$

$$\tau_{\alpha Z\beta\zeta}^{(Zh)} = \frac{n_{\alpha Z}}{n_\alpha}\frac{\tau_{\alpha\beta}^{(Zh)}}{I_{\alpha Z} I_{\beta\zeta}}, \quad \tau_\alpha^{(Zh)} = \left(\sum_\beta \frac{\mu_{\alpha\beta}}{m_\alpha \tau_{\alpha\beta}^{(Zh)}}\right)^{-1}. \tag{A17}$$

Z-variables are defined by

$$Z_\alpha^* = \sum_{\beta\neq\alpha}\frac{\overline{Z_\beta^2} n_\beta}{\overline{Z_\alpha^2} n_\alpha}, \quad Z_{c\alpha}^* = \sum_{\beta\neq\alpha}\sqrt{\frac{\mu_{\alpha\beta}}{m_\alpha}}\frac{\overline{Z_\beta^2} n_\beta}{\overline{Z_\alpha^2} n_\alpha}, \tag{A18}$$

$$Z_{f1\alpha}^* = Z_{2\alpha}^s = \sum_{\beta\neq\alpha}\left(\frac{\mu_{\alpha\beta}}{m_\alpha}\right)^{3/2}\frac{\overline{Z_\beta^2} n_\beta}{\overline{Z_\alpha^2} n_\alpha}, \tag{A19}$$

$$Z_{f2\alpha}^* = Z_{8\alpha}^s = \sum_{\beta\neq\alpha}\left(\frac{\mu_{\alpha\beta}}{m_\alpha}\right)^{5/2}\frac{\overline{Z_\beta^2} n_\beta}{\overline{Z_\alpha^2} n_\alpha}, \tag{A20}$$

$$Z_{11\alpha}^* = Z_{5\alpha}^s = \sum_{\beta\neq\alpha}\left(1 + \frac{16}{13}\frac{m_\alpha}{m_\beta} + \frac{30}{13}\left(\frac{m_\alpha}{m_\beta}\right)^2\right)\left(\frac{\mu_{\alpha\beta}}{m_\alpha}\right)^{5/2}\frac{\overline{Z_\beta^2} n_\beta}{\overline{Z_\alpha^2} n_\alpha}, \tag{A21}$$

$$Z_{12\alpha}^* = Z_{9\alpha}^s = \sum_{\beta\neq\alpha}\left(1 + \frac{32}{23}\frac{m_\alpha}{m_\beta} + \frac{84}{23}\left(\frac{m_\alpha}{m_\beta}\right)^2\right)\left(\frac{\mu_{\alpha\beta}}{m_\alpha}\right)^{7/2}\frac{\overline{Z_\beta^2} n_\beta}{\overline{Z_\alpha^2} n_\alpha}, \tag{A22}$$

$$Z^*_{22\alpha}=Z^s_{11\alpha}=\sum_{\beta\neq\alpha}\Bigg(1+\frac{1088}{433}\frac{m_\alpha}{m_\beta}+\frac{3672}{433}\left(\frac{m_\alpha}{m_\beta}\right)^2+\frac{1792}{433}\left(\frac{m_\alpha}{m_\beta}\right)^3+\frac{1400}{433}\left(\frac{m_\alpha}{m_\beta}\right)^4\Bigg)\left(\frac{\mu_{\alpha\beta}}{m_\alpha}\right)^{9/2}\frac{\overline{Z^2_\beta}n_\beta}{\overline{Z^2_\alpha}n_\alpha},\quad(A23)$$

$$Z^\pi_{11\alpha}=\sum_{\beta\neq\alpha}\left(1+\frac{5}{3}\frac{m_\alpha}{m_\beta}\right)\left(\frac{\mu_{\alpha\beta}}{m_\alpha}\right)^{3/2}\frac{\overline{Z^2_\beta}n_\beta}{\overline{Z^2_\alpha}n_\alpha},\quad(A24)$$

$$Z^\pi_{12\alpha}=\sum_{\beta\neq\alpha}\left(1+\frac{7}{3}\frac{m_\alpha}{m_\beta}\right)\left(\frac{\mu_{\alpha\beta}}{m_\alpha}\right)^{5/2}\frac{\overline{Z^2_\beta}n_\beta}{\overline{Z^2_\alpha}n_\alpha},\quad(A25)$$

$$Z^\pi_{22\alpha}=\sum_{\beta\neq\alpha}\left(1+\frac{185}{51}\frac{m_\alpha}{m_\beta}+\frac{154}{51}\left(\frac{m_\alpha}{m_\beta}\right)^2+\frac{140}{51}\left(\frac{m_\alpha}{m_\beta}\right)^3\right)\times\left(\frac{\mu_{\alpha\beta}}{m_\alpha}\right)^{7/2}\frac{\overline{Z^2_\beta}n_\beta}{\overline{Z^2_\alpha}n_\alpha}.\quad(A26)$$

Note: If $m_\alpha/m_\beta\to 0$, all Z-variables become equal to Z^*_α.

2. Results

The results in this section are presented for the parallel (with regard to the B-field) component (the heat flux, r-moment, and friction term are written in a vector form to be applied in case $B=0$ for all components).

a. Heat flux

Averaged over all charge states,

$$\bar{\mathbf{h}}_\alpha=-\frac{p_\alpha n_\alpha}{\lambda_{\alpha\alpha}}c^{(h^A_T)}_\alpha\widetilde{\nabla T_\alpha}+p_\alpha\sum_\beta c^{(h^A_w)}_{\beta\alpha}(\bar{\mathbf{w}}_\alpha-\bar{\mathbf{w}}_\beta),\quad(A27)$$

where

$$c^{(h^A_w)}_{\beta\alpha}=\frac{25}{16}\frac{\mu_{\alpha\beta}}{m_\alpha}\frac{1}{\widetilde{\Delta}_\alpha}\sqrt{2}\sqrt{\frac{\mu_{\alpha\beta}}{m_\alpha}\frac{\overline{Z^2_\beta}n_\beta}{\overline{Z^2_\alpha}n_\alpha}}\left(\frac{3}{2}-\frac{1}{2}\frac{\mu_{\alpha\beta}}{m_\alpha}+\frac{433\sqrt{2}}{240}Z^*_{22\alpha}-\frac{23\sqrt{2}}{16}\frac{\mu_{\alpha\beta}}{m_\alpha}Z^*_{12\alpha}\right),\quad(A28)$$

$$c^{(h^A_T)}_\alpha=\frac{125}{32}\frac{1}{\widetilde{\Delta}_\alpha}\left(1+\frac{433\sqrt{2}}{360}Z^*_{22\alpha}\right),\quad(A29)$$

$$\widetilde{\Delta}_\alpha=\frac{5629}{1152}Z^*_{11\alpha}Z^*_{22\alpha}-\frac{529}{128}{Z^*_{12\alpha}}^2+\frac{65\sqrt{2}}{32}Z^*_{11\alpha}+\frac{433\sqrt{2}}{288}Z^*_{22\alpha}-\frac{23\sqrt{2}}{16}Z^*_{12\alpha}+1.\quad(A30)$$

Note, in the $m_\alpha/m_\beta\to 0$ limit, $Z^*_{c\alpha}=Z^*_{11\alpha}=Z^*_{12\alpha}=Z^*_{22\alpha}=Z^*_\alpha$ and these expressions turn into (8.4.7) in Ref. 1.

For each charge state,

$$\mathbf{h}_{\alpha Z}=\mathbf{h}^T_{\alpha Z}+\mathbf{h}^{\mathbf{w}}_{\alpha Z},\quad(A31)$$

$$\mathbf{h}^T_{\alpha Z}=-\frac{p_{\alpha Z}n_\alpha}{\lambda_{\alpha\alpha}}c^{(h^A_T)}_\alpha\widetilde{\nabla T_\alpha}-\frac{p_{\alpha Z}n_\alpha}{\lambda_{\alpha\alpha}}c^{(h^B_T)}_\alpha\left(\frac{\overline{Z^2_\alpha}}{Z^2}\nabla T_{\alpha Z}-\widetilde{\nabla T_\alpha}\right),\quad(A32)$$

$$\mathbf{h}^{\mathbf{w}}_{\alpha Z}=p_{\alpha Z}\sum_\beta c^{(h^A_w)}_{\beta\alpha}(\bar{\mathbf{w}}_\alpha-\bar{\mathbf{w}}_\beta)+p_{\alpha Z}c^{(h^B_w)}_\alpha(\mathbf{w}_{\alpha Z}-\bar{\mathbf{w}}_\alpha)=p_{\alpha Z}\sum_\beta c^{(h_w)}_{\beta\alpha}(\mathbf{w}_{\alpha Z}-\bar{\mathbf{w}}_\beta),\quad(A33)$$

where

$$c^{(h^B_T)}_\alpha=-\frac{5}{2}\frac{S^{(11)}_\alpha\lambda_{\alpha\alpha}}{D_\alpha}=\frac{139750}{53471}\frac{1+\frac{6928\sqrt{2}}{8385}Z^s_{11\alpha}}{D^{part}_\alpha},\quad(A34)$$

$$c^{(h^B_w)}_\alpha=\frac{S^{(9)}_\alpha S^{(8)}_\alpha-S^{(2)}_\alpha S^{(11)}_\alpha}{D_\alpha}=\frac{31500}{53471}\frac{1}{D^{part}_\alpha}\left(1-\frac{139\sqrt{2}}{105}Z^s_{8\alpha}-\frac{46\sqrt{2}}{105}Z^s_{9\alpha}+\frac{1732\sqrt{2}}{1575}Z^s_{11\alpha}+\frac{559\sqrt{2}}{210}Z^s_{2\alpha}-\frac{368}{105}Z^s_{8\alpha}Z^s_{9\alpha}+\frac{6928}{1575}Z^s_{2\alpha}Z^s_{11\alpha}\right),\quad(A35)$$

$$D^{part}_\alpha=\frac{89600}{160413}\frac{D_\alpha}{\lambda^2_{\alpha\alpha}}=1+\frac{204376\sqrt{2}}{160413}Z^s_{11\alpha}+\frac{72670\sqrt{2}}{53471}Z^s_{5\alpha}-\frac{76728\sqrt{2}}{53471}Z^s_{9\alpha}+\frac{360256}{160413}Z^s_{5\alpha}Z^s_{11\alpha}-\frac{101568}{53471}(Z^s_{9\alpha})^2,\quad(A36)$$

$$c^{(h_w)}_{\beta\alpha}=\delta_{\alpha\beta}c^{(h^B_w)}_\beta-\delta_{\alpha\beta}\sum_\gamma c^{(h^A_w)}_{\gamma\alpha}+c^{(h^A_w)}_{\beta\alpha},\quad(A37)$$

where $\delta_{\alpha\beta}$ is the Kronecker delta.

b. R-moment

The r-moment is an additional vector moment, see Eq. (8.1.2) in Ref. 1.

Averaged over all charge states,

$$\bar{\mathbf{r}}_\alpha=-\frac{p_\alpha n_\alpha}{\lambda_{\alpha\alpha}}c^{(r^A_T)}_\alpha\frac{T}{m_\alpha}\widetilde{\nabla T_\alpha}+p_\alpha\frac{T}{m_\alpha}\sum_\beta c^{(r^A_w)}_{\beta\alpha}(\bar{\mathbf{w}}_\alpha-\bar{\mathbf{w}}_\beta),\quad(A38)$$

where

$$c^{(r^A_w)}_{\beta\alpha}=-\frac{35}{24}\frac{\mu_{\alpha\beta}}{m_\alpha}\frac{1}{\widetilde{\Delta}_\alpha}\sqrt{2}\sqrt{\frac{\mu_{\alpha\beta}}{m_\alpha}\frac{\overline{Z^2_\beta}n_\beta}{\overline{Z^2_\alpha}n_\alpha}}\left(\frac{5}{2}\frac{\mu_{\alpha\beta}}{m_\alpha}-\frac{3}{2}+\frac{65\sqrt{2}}{16}\frac{\mu_{\alpha\beta}}{m_\alpha}Z^*_{11\alpha}-\frac{69\sqrt{2}}{16}Z^*_{12\alpha}\right),\quad(A39)$$

$$c^{(r^A_T)}_\alpha=\frac{175}{48}\frac{1}{\widetilde{\Delta}_\alpha}\left(1+\frac{23\sqrt{2}}{8}Z^*_{12\alpha}\right).\quad(A40)$$

For each charge state,

$$\mathbf{r}_{\alpha Z}=\mathbf{r}^T_{\alpha Z}+\mathbf{r}^{\mathbf{w}}_{\alpha Z},\quad(A41)$$

$$\mathbf{r}^T_{\alpha Z}=-\frac{p_{\alpha Z}n_\alpha}{\lambda_{\alpha\alpha}}c^{(r^A_T)}_\alpha\frac{T}{m_\alpha}\widetilde{\nabla T_\alpha}-\frac{p_{\alpha Z}n_\alpha}{\lambda_{\alpha\alpha}}c^{(r^B_T)}_\alpha\frac{T}{m_\alpha}\left(\frac{\overline{Z^2_\alpha}}{Z^2}\nabla T_{\alpha Z}-\widetilde{\nabla T_\alpha}\right),\quad(A42)$$

$$\mathbf{r}^{\mathbf{w}}_{\alpha Z}=p_{\alpha Z}\frac{T}{m_\alpha}\sum_\beta c^{(r^A_w)}_{\beta\alpha}(\bar{\mathbf{w}}_\alpha-\bar{\mathbf{w}}_\beta)+p_{\alpha Z}\frac{T}{m_\alpha}c^{(r^B_w)}_\alpha(\mathbf{w}_{\alpha Z}-\bar{\mathbf{w}}_\alpha)=p_{\alpha Z}\frac{T}{m_\alpha}\sum_\beta c^{(r_w)}_{\beta\alpha}(\mathbf{w}_{\alpha Z}-\bar{\mathbf{w}}_\beta),\quad(A43)$$

where

$$c_\alpha^{(r_T^B)} = \frac{35}{2}\frac{S_\alpha^{(9)}\lambda_{\alpha\alpha}}{D_\alpha} = \frac{194600}{53471}\frac{1+\frac{184\sqrt{2}}{139}Z_{9\alpha}^s}{D_\alpha^{part}}, \tag{A44}$$

$$c_\alpha^{(r_w^B)} = \frac{7S_\alpha^{(2)}S_\alpha^{(9)} - S_\alpha^{(5)}S_\alpha^{(8)}}{D_\alpha}$$
$$= \frac{17080}{53471}\frac{1}{D_\alpha^{part}}\left(1+\frac{276\sqrt{2}}{61}Z_{9\alpha}^s + \frac{417\sqrt{2}}{61}Z_{2\alpha}^s - \frac{590\sqrt{2}}{61}Z_{8\alpha}^s - \frac{130\sqrt{2}}{61}Z_{5\alpha}^s + \frac{1104}{61}Z_{2\alpha}^sZ_{9\alpha}^s - \frac{1040}{61}Z_{5\alpha}^sZ_{8\alpha}^s\right), \tag{A45}$$

$$c_{\beta\alpha}^{(r_w)} = \delta_{\alpha\beta}c_\beta^{(r_w^B)} - \delta_{\alpha\beta}\sum_\gamma c_{\gamma\alpha}^{(r_w^A)} + c_{\beta\alpha}^{(r_w^A)}, \tag{A46}$$

where $\delta_{\alpha\beta}$ is the Kronecker delta.

c. Friction term

Friction terms can be split into thermal force and friction force components

$$\mathbf{R}_{\alpha Z} = \mathbf{R}_{\alpha Z}^T + \mathbf{R}_{\alpha Z}^{\mathbf{w}}. \tag{A47}$$

Thermal force averaged over all charge states,

$$\mathbf{R}_\alpha^T = -\sum_{\beta\neq\alpha}\left[n_\alpha c_{\alpha\beta}^{(R_T^A)}\frac{\overline{Z_\beta^2}n_\beta}{\overline{Z_\alpha^2}n_\alpha}\widetilde{\nabla T_\alpha} - n_\beta c_{\beta\alpha}^{(R_T^A)}\frac{\overline{Z_\alpha^2}n_\alpha}{\overline{Z_\beta^2}n_\beta}\widetilde{\nabla T_\beta}\right], \tag{A48}$$

where

$$c_{\alpha\beta}^{(R_T^A)} = \frac{1}{\widetilde{\Delta}_\alpha}\frac{25\sqrt{2}}{16}\left(\frac{\mu_{\alpha\beta}}{m_\alpha}\right)^{3/2}\left[\frac{3}{2}\left(1+\frac{433\sqrt{2}}{360}Z_{22\alpha}^*\right) - \frac{1}{2}\frac{\mu_{\alpha\beta}}{m_\alpha}\left(1+\frac{23\sqrt{2}}{8}Z_{12\alpha}^*\right)\right]. \tag{A49}$$

If $m_\alpha/m_\beta \to 0$, $Z_{f1\alpha}^* = Z_{f2\alpha}^* = Z_{c\alpha}^* = Z_{11\alpha}^* = Z_{12\alpha}^* = Z_{22\alpha}^* = Z_\alpha^*$ and

$$\sum_{\beta\neq\alpha}c_{\alpha\beta}^{(R_T^A)}\frac{\overline{Z_\beta^2}n_\beta}{\overline{Z_\alpha^2}n_\alpha} = \frac{25\sqrt{2}}{16}\frac{1}{\Delta_\alpha}Z_\alpha^*\left(1+\frac{11\sqrt{2}}{30}Z_\alpha^*\right), \tag{A50}$$

which matches the corresponding (8.4.7) in Ref. 1.

For each charge state,

$$\mathbf{R}_{\alpha Z}^T = -n_{\alpha Z}\frac{Z^2}{\overline{Z_\alpha^2}}\sum_{\beta\neq\alpha}\left[c_{\alpha\beta}^{(R_T^A)}\frac{\overline{Z_\beta^2}n_\beta}{\overline{Z_\alpha^2}n_\alpha}\widetilde{\nabla T_\alpha} - \frac{n_\beta}{n_\alpha}c_{\beta\alpha}^{(R_T^A)}\frac{\overline{Z_\alpha^2}n_\alpha}{\overline{Z_\beta^2}n_\beta}\widetilde{\nabla T_\beta}\right] - n_{\alpha Z}c_\alpha^{(R_T^B)}\left(\nabla T_{\alpha Z} - \frac{Z^2}{\overline{Z_\alpha^2}}\widetilde{\nabla T_\alpha}\right), \tag{A51}$$

where

$$c_\alpha^{(R_T^B)} = \frac{3}{5}c_\alpha^{(h_T^B)}\left(\frac{1}{2}+\sqrt{2}Z_{f1\alpha}^*\right) - \frac{3}{14}c_\alpha^{(r_T^B)}\left(\frac{1}{4}+\sqrt{2}Z_{f2\alpha}^*\right)$$
$$= \frac{31500}{53471}\frac{1}{D_\alpha^{part}}\left[\frac{559}{420}\left(1+\frac{6928\sqrt{2}}{8385}Z_{11\alpha}^s\right)\left(1+2\sqrt{2}Z_{f1\alpha}^*\right) - \frac{139}{420}\left(1+\frac{184\sqrt{2}}{139}Z_{9\alpha}^s\right)\left(1+4\sqrt{2}Z_{f2\alpha}^*\right)\right]. \tag{A52}$$

Friction force averaged over all charge states,

$$\mathbf{R}_\alpha^{\mathbf{w}} = -n_\alpha\sum_\beta\frac{\mu_{\alpha\beta}}{\tau_{\alpha\beta}^{(Zh)}}c_{\beta\alpha}^{(R_w^A)}(\bar{\mathbf{w}}_\alpha - \bar{\mathbf{w}}_\beta), \tag{A53}$$

where

$$c_{\beta\alpha}^{(R_w^A)} = 1 + c_{\beta\alpha}^{(R_w^A1)} + c_{\beta\alpha}^{(R_w^A2)} + c_{\beta\alpha}^{(R_w^A3)}, \tag{A54}$$

$$c_{\beta\alpha}^{(R_w^A1)} = -\sum_{\gamma\neq\alpha}\frac{\mu_{\alpha\gamma}}{m_\alpha}\sqrt{\frac{\mu_{\alpha\gamma}}{\mu_{\alpha\beta}}\frac{\overline{Z_\gamma^2}n_\gamma}{\overline{Z_\beta^2}n_\beta}}\left[\frac{3}{5}c_{\beta\alpha}^{(h_w^A)} - \frac{3}{14}\frac{\mu_{\alpha\gamma}}{m_\alpha}c_{\beta\alpha}^{(r_w^A)}\right], \tag{A55}$$

$$c_{\beta\alpha}^{(R_w^A2)} = \sum_{\gamma\neq\alpha}\frac{\mu_{\alpha\gamma}}{m_\gamma}\sqrt{\frac{\mu_{\alpha\gamma}}{\mu_{\alpha\beta}}\frac{\overline{Z_\gamma^2}n_\gamma}{\overline{Z_\beta^2}n_\beta}}\left[\frac{3}{5}c_{\beta\gamma}^{(h_w^A)} - \frac{3}{14}\frac{\mu_{\alpha\gamma}}{m_\gamma}c_{\beta\gamma}^{(r_w^A)}\right], \tag{A56}$$

$$c_{\beta\alpha}^{(R_w^A3)} = -\frac{\mu_{\alpha\beta}}{m_\beta}\sum_\gamma\left[\frac{3}{5}c_{\gamma\beta}^{(h_w^A)} - \frac{3}{14}\frac{\mu_{\alpha\beta}}{m_\beta}c_{\gamma\beta}^{(r_w^A)}\right]. \tag{A57}$$

Note

$$1 + c_{\beta\alpha}^{(R_w^A1)} = 1 - \frac{15\sqrt{2}}{16}Z_{f1\alpha}^*\frac{\mu_{\alpha\beta}}{m_\alpha}\frac{1}{\widetilde{\Delta}_\alpha}\left(\frac{3}{2} - \frac{1}{2}\frac{\mu_{\alpha\beta}}{m_\alpha} + \frac{433\sqrt{2}}{240}Z_{22\alpha}^* - \frac{23\sqrt{2}}{16}\frac{\mu_{\alpha\beta}}{m_\alpha}Z_{12\alpha}^*\right) - \frac{5\sqrt{2}}{16}Z_{f2\alpha}^*\frac{\mu_{\alpha\beta}}{m_\alpha}\frac{1}{\widetilde{\Delta}_\alpha} \times\left(\frac{5}{2}\frac{\mu_{\alpha\beta}}{m_\alpha} - \frac{3}{2} + \frac{65\sqrt{2}}{16}\frac{\mu_{\alpha\beta}}{m_\alpha}Z_{11\alpha}^* - \frac{69\sqrt{2}}{16}Z_{12\alpha}^*\right). \tag{A58}$$

In the $m_\alpha/m_\beta \to 0$ limit, $Z_{f1\alpha}^* = Z_{f2\alpha}^* = Z_{c\alpha}^* = Z_{11\alpha}^* = Z_{12\alpha}^* = Z_{22\alpha}^* = Z_\alpha^*$ and

$$c_{\beta\alpha}^{(R_w^A)} = 1 + c_{\beta\alpha}^{(R_w^A1)} = c_{\beta\alpha}^{(1)} = \frac{1}{\Delta_\alpha}\left(\frac{2}{9}Z_\alpha^{*2} + \frac{61\sqrt{2}}{72}Z_\alpha^* + 1\right), \tag{A59}$$

which matches with (8.4.7) in Ref. 1.

For each charge state,

$$\mathbf{R}_{\alpha Z}^{\mathbf{w}} = -n_\alpha I_{\alpha Z}\sum_\beta\frac{\mu_{\alpha\beta}}{\tau_{\alpha\beta}^{(Zh)}}c_{\beta\alpha}^{(R_w^A)}(\bar{\mathbf{w}}_\alpha - \bar{\mathbf{w}}_\beta) - n_\alpha I_{\alpha Z}(\mathbf{w}_{\alpha Z} - \bar{\mathbf{w}}_\alpha)\sum_\beta\frac{\mu_{\alpha\beta}}{\tau_{\alpha\beta}^{(Zh)}}c_{\beta\alpha}^{(R_w^B)}$$
$$= -n_\alpha I_{\alpha Z}\sum_\beta\frac{\mu_{\alpha\beta}}{\tau_{\alpha\beta}^{(Zh)}}c_{\beta\alpha}^{(R_w)}(\mathbf{w}_{\alpha Z} - \bar{\mathbf{w}}_\beta), \tag{A60}$$

$$c_{\beta\alpha}^{(R_w^B)} = 1 - \frac{3}{5}\frac{\mu_{\alpha\beta}}{m_\alpha}c_\alpha^{(h_w^B)} + \frac{3}{14}\left(\frac{\mu_{\alpha\beta}}{m_\alpha}\right)^2c_\alpha^{(r_w^B)}, \tag{A61}$$

$$c_{\beta\alpha}^{(R_w)} = \delta_{\alpha\beta}\sum_\gamma\sqrt{\frac{\mu_{\alpha\gamma}}{\mu_{\alpha\beta}}\frac{\overline{Z_\gamma^2}n_\gamma}{\overline{Z_\beta^2}n_\beta}}\left[c_{\gamma\alpha}^{(R_w^B)} - c_{\gamma\alpha}^{(R_w^A)}\right] + c_{\beta\alpha}^{(R_w^A)}, \tag{A62}$$

where $\delta_{\alpha\beta}$ is the Kronecker delta.

d. Viscous stress tensor

Averaged over all charge states,

$$\bar{\pi}_{\alpha|||} = -\frac{m_\alpha n_\alpha}{\lambda_{\alpha\alpha}}c_\alpha^{(\pi_u^A)}p_\alpha W_{|||} - \frac{m_\alpha n_\alpha}{\lambda_{\alpha\alpha}}c_\alpha^{(\pi_h^A)}W_{|||}^{\bar{h}_a}, \tag{A63}$$

where

$$\Delta_\alpha^\pi = \frac{204}{89} Z_{11\alpha}^\pi Z_{22\alpha}^\pi - \frac{108}{89} {Z_{12\alpha}^\pi}^2 + \frac{205\sqrt{2}}{178} Z_{11\alpha}^\pi + \frac{102\sqrt{2}}{89} Z_{22\alpha}^\pi - \frac{54\sqrt{2}}{89} Z_{12\alpha}^\pi + 1, \tag{A64}$$

$$c_\alpha^{(\pi_u^A)} = \frac{1025}{1068} \frac{1}{\Delta_\alpha^\pi} \left(1 + \frac{204\sqrt{2}}{205} Z_{22\alpha}^\pi\right), \tag{A65}$$

$$c_\alpha^{(\pi_h^A)} = \frac{1655}{1068} \frac{1}{\Delta_\alpha^\pi} \left(1 + \frac{204\sqrt{2}}{331} Z_{22\alpha}^\pi + \frac{252\sqrt{2}}{331} Z_{12\alpha}^\pi\right). \tag{A66}$$

If $m_\alpha/m_\beta \to 0$, $Z_{c\alpha}^* = Z_{11\alpha}^\pi = Z_{12\alpha}^\pi = Z_{22\alpha}^\pi = Z_\alpha^*$ and

$$\left(1 + \sqrt{2} Z_{c\alpha}^*\right) c_\alpha^{(\pi_u^A)} = \frac{1025}{1068} \frac{\left(1 + \sqrt{2} Z_\alpha^*\right)\left(1 + \frac{204\sqrt{2}}{205} Z_\alpha^*\right)}{\frac{96}{89} Z_\alpha^{*2} + \frac{301\sqrt{2}}{178} Z_\alpha^* + 1}, \tag{A67}$$

which matches the last expression on p. 181 of Ref. 1.

For each charge state,

$$\pi_{\alpha Z|||} = \pi_{\alpha Z|||}^u + \pi_{\alpha Z|||}^h, \tag{A68}$$

$$\pi_{\alpha Z|||}^u = -\frac{m_\alpha n_{\alpha Z} n_\alpha T}{\lambda_{\alpha\alpha}} \left[c_\alpha^{(\pi_u^A)} + c_\alpha^{(\pi_u^B)} \left(\frac{\overline{Z_\alpha^2}}{Z^2} - 1\right)\right] W_{|||}, \tag{A69}$$

$$\pi_{\alpha Z|||}^h = -\frac{m_\alpha n_{\alpha Z}}{\lambda_{\alpha\alpha}} \left[c_\alpha^{(\pi_h^A)} W_{|||}^{\bar{h}_a} + c_\alpha^{(\pi_h^B)} \left(\frac{\overline{Z_\alpha^2} n_\alpha}{Z^2 n_{\alpha Z}} W_{|||}^{h_{\alpha Z}} - W_{|||}^{\bar{h}_\alpha}\right)\right], \tag{A70}$$

where

$$c_\alpha^{(\pi_u^B)} = -\lambda_{\alpha\alpha} \frac{S_\alpha^{(15)}}{D_\alpha^\pi} = \frac{265}{334} \frac{1 + \frac{204\sqrt{2}}{265} Z_{22\alpha}^\pi}{D_\alpha^{\pi part}}, \tag{A71}$$

$$c_\alpha^{(\pi_h^B)} = -\lambda_{\alpha\alpha} \frac{S_\alpha^{(15)} - \frac{7}{2} S_\alpha^{(13)}}{D_\alpha^\pi} = \frac{475}{334} \frac{1 + \frac{252\sqrt{2}}{475} Z_{12\alpha}^\pi + \frac{204\sqrt{2}}{475} Z_{22\alpha}^\pi}{D_\alpha^{\pi part}}, \tag{A72}$$

$$D_\alpha^{\pi part} = \frac{70}{167} \frac{D_\alpha^\pi}{\lambda_{\alpha\alpha}^2} = 1 + \frac{159\sqrt{2}}{167} Z_{11\alpha}^\pi + \frac{816\sqrt{2}}{835} Z_{22\alpha}^\pi - \frac{108\sqrt{2}}{167} Z_{12\alpha}^\pi + \frac{1224}{835} Z_{11\alpha}^\pi Z_{22\alpha}^\pi - \frac{648}{835} (Z_{12\alpha}^\pi)^2. \tag{A73}$$

3. S-coefficients

This section gives coefficients used for results in Subsection 2 "Results". They are used in Refs. 1, 6, and 12. These coefficients are obtained without additional assumptions; therefore, they must match exactly the corresponding in Refs. 1, 6, and 12.

For the heat flux,

$$S_\alpha^{(2)} = \sum_\beta \frac{5}{2} \frac{\mu_{\alpha\beta}}{m_\alpha} \bar{G}_{\alpha\beta}^{(2)} = \lambda_{\alpha\alpha} \left[\frac{3}{4} + \frac{3\sqrt{2}}{2} Z_{2\alpha}^s\right], \tag{A74}$$

$$S_\alpha^{(5)} = \sum_\beta \bar{G}_{\alpha\beta}^{(5)} = -\lambda_{\alpha\alpha} \left[\frac{59}{40} + \frac{13\sqrt{2}}{10} Z_{5\alpha}^s\right], \tag{A75}$$

$$S_\alpha^{(8)} = \sum_\beta \frac{35}{2} \left(\frac{\mu_{\alpha\beta}}{m_\alpha}\right)^2 \bar{G}_{\alpha\beta}^{(8)} = -\lambda_{\alpha\alpha} \left[\frac{15}{16} + \frac{15\sqrt{2}}{4} Z_{8\alpha}^s\right], \tag{A76}$$

$$S_\alpha^{(9)} = \sum_\beta \frac{\mu_{\alpha\beta}}{m_\alpha} \bar{G}_{\alpha\beta}^{(9)} = \lambda_{\alpha\alpha} \left[\frac{417}{1120} + \frac{69\sqrt{2}}{140} Z_{9\alpha}^s\right], \tag{A77}$$

$$S_\alpha^{(11)} = \sum_\beta \bar{G}_{\alpha\beta}^{(11)} = -\lambda_{\alpha\alpha} \left[\frac{1677}{896} + \frac{433\sqrt{2}}{280} Z_{11\alpha}^s\right], \tag{A78}$$

$$D_\alpha = S_\alpha^{(5)} S_\alpha^{(11)} - 7 (S_\alpha^{(9)})^2. \tag{A79}$$

For viscous stress tensor,

$$S_\alpha^{(3)} = \sum_\beta \frac{m_\alpha}{m_\alpha + m_\beta} \bar{G}_{\alpha\beta}^{(3)} = -\lambda_{\alpha\alpha} \left[\frac{8}{5} + \frac{6\sqrt{2}}{5} Z_{11\alpha}^\pi\right], \tag{A80}$$

$$S_\alpha^{(13)} = \sum_\beta \frac{\mu_{\alpha\beta}}{m_\alpha + m_\beta} \bar{G}_{\alpha\beta}^{(13)} = \lambda_{\alpha\alpha} \left[\frac{3}{7} + \frac{18\sqrt{2}}{35} Z_{12\alpha}^\pi\right], \tag{A81}$$

$$S_\alpha^{(15)} = \sum_\beta \frac{m_\alpha}{m_\alpha + m_\beta} \bar{G}_{\alpha\beta}^{(15)} = -\lambda_{\alpha\alpha} \left[\frac{53}{28} + \frac{51\sqrt{2}}{35} Z_{22\alpha}^\pi\right], \tag{A82}$$

$$D_\alpha^\pi = S_\alpha^{(3)} S_\alpha^{(15)} - \frac{7}{2} \left(S_\alpha^{(13)}\right)^2. \tag{A83}$$

APPENDIX B: VISCOUS STRESS TENSOR DIVERGENCE IN THE MULTICOMPONENT PLASMA

This appendix considers the study of the divergence $\nabla \cdot \overleftrightarrow{\pi}_{\alpha Z}^{(par)}$, taking into account parallel and drift components of the velocity and parallel and diamagnetic components of the heat flux.

The parallel component of the viscous stress tensor (28) in an arbitrary coordinate system is

$$\pi_{\alpha Z}^{(par)}{}_{kl} = -\frac{3}{2} \left(b_k b_l - \frac{1}{3} \delta_{kl}\right) \times \left[\frac{n_{\alpha Z}}{n_\alpha} \left(\sum_\beta \left[\tilde{c}_{\alpha\beta}^{(\pi_u^A)} + 2 c_\alpha^{(\pi_u^B)} \frac{\overline{Z_\alpha^2}}{Z^2} \delta_{\alpha\beta}\right] \tau_{\beta\alpha}^{(Zh)} p_\beta\right) W_{|||} + \frac{n_{\alpha Z}}{n_\alpha} \sum_\beta \left(\tilde{c}_{\alpha\beta}^{(\pi_h^A)} \tau_{\beta\alpha}^{(Zh)} W_{|||}^{\bar{h}_\beta}\right) + 2 c_\alpha^{(\pi_h^B)} \frac{\overline{Z_\alpha^2}}{Z^2} \tau_{\alpha\alpha}^{(Zh)} W_{|||}^{h_{\alpha Z}}\right], \tag{B1}$$

where $\mathbf{b} = \mathbf{B}/B$ and for $\mathbf{u}$ we substitute into $W_{|||}$ the sum of the parallel velocity, $E \times B$ and diamagnetic velocities,

$$\mathbf{u} = \mathbf{b} \cdot \frac{1}{\rho} \sum_{\beta,\zeta} m_\beta n_{\beta\zeta} u_{\beta\zeta\|} + \mathbf{u}^{\text{dia}} + \mathbf{u}^{E\times B}, \tag{B2}$$

$$\mathbf{u}^{\text{dia}} = \frac{1}{\rho B^2} \left[\mathbf{B} \times \nabla \sum_{\beta,\zeta} \left(\frac{m_\beta n_{\beta\zeta} T_{\beta\zeta}}{\zeta e}\right)\right], \tag{B3}$$

$$\mathbf{u}^{E\times B} = \frac{1}{B^2} [\mathbf{B} \times \nabla\varphi], \tag{B4}$$

where summation is over all ions β with charge states ζ and

$$u_{\beta\zeta\|} = (\mathbf{b} \cdot \mathbf{u}_{\beta\zeta}), \quad \rho = \sum_{\beta,\zeta} m_\beta n_{\beta\zeta}.$$

For $\bar{\mathbf{h}}_\alpha$ we substitute into $W_{|||}^{\bar{h}_a}$ [using (A3)], and for $\mathbf{h}_{\alpha Z}$ we substitute into $W_{|||}^{h_{\alpha Z}}$

$$\mathbf{h}_{\alpha Z} = \mathbf{b}\cdot h_{\alpha Z\parallel} + \mathbf{h}^{(dia)}_{\alpha Z\perp}, \tag{B5}$$

where [see Eq. (8.3.1) in Ref. 1]

$$\mathbf{h}^{(dia)}_{\alpha Z\perp} = -\frac{5}{2}\frac{p_{\alpha Z}[\nabla T_{\alpha Z}\times\mathbf{B}]}{ZeB^2}. \tag{B6}$$

Making use of

$$(\vec{\mathbf{B}}\cdot\nabla)\vec{\mathbf{B}} = \frac{1}{2}\nabla B^2 - [\vec{\mathbf{B}}\times[\nabla\times\vec{\mathbf{B}}]] \approx \frac{1}{2}\nabla B^2$$

one finally gets

$$\begin{aligned}(\nabla\cdot\overleftrightarrow{\pi}^{(par)}_{\alpha Z})_\parallel = &-\frac{2}{3}B^{3/2}\nabla_\parallel\left[\frac{n_{\alpha Z}}{n_\alpha}\left[\sum_\beta \tilde{c}^{(\pi^A_u)}_{\alpha\beta}\tau^{(Zh)}_{\beta\alpha}p_\beta\right.\right.\\ &\left.+2c^{(\pi^B_u)}_\alpha\tau^{(Zh)}_{\alpha\alpha}\frac{\overline{Z^2_\alpha}}{Z^2}p_\alpha\right]*\left[\frac{1}{B^2}\nabla_\parallel\left(2\sqrt{B}u_\parallel\right)\right.\\ &\left.-(\mathbf{u}^{E\times B}+\mathbf{u}^{\rm dia})\cdot\frac{\nabla B}{B^{5/2}}+\mathbf{u}^{\rm dia}\cdot\frac{1}{B^{3/2}}\frac{\nabla\rho}{\rho}\right]\Bigg]\\ &-\frac{4}{15}B^{3/2}\nabla_\parallel\left[\frac{n_{\alpha Z}}{n_\alpha}\left[\sum_\beta\left(\tilde{c}^{(\pi^A_h)}_{\alpha\beta}\tau^{(Zh)}_{\beta\alpha}\left(\frac{1}{B^2}\nabla_\parallel\left(2\sqrt{B}\bar{h}_{\beta\parallel}\right)\right.\right.\right.\right.\\ &\left.\left.\left.\left.-\bar{\mathbf{h}}^{dia}_{\beta\perp}\cdot\frac{\nabla B}{B^{5/2}}-\bar{\mathbf{h}}^{dia}_{\beta\perp}\cdot\frac{1}{B^{3/2}}\frac{\nabla p_\beta}{p_\beta}\right)\right)\right.\\ &+2c^{(\pi^B_h)}_\alpha\tau^{(Zh)}_{\alpha\alpha}\frac{\overline{Z^2_\alpha}n_\alpha}{Z^2n_{\alpha Z}}\left(\frac{1}{B^2}\nabla_\parallel\left(2\sqrt{B}h_{\alpha Z\parallel}\right)\right.\\ &\left.\left.-\mathbf{h}^{dia}_{\alpha Z\perp}\cdot\frac{\nabla B}{B^{5/2}}-\mathbf{h}^{dia}_{\alpha Z\perp}\cdot\frac{1}{B^{3/2}}\frac{\nabla p_{\alpha Z}}{p_{\alpha Z}}\right)\right]\Bigg].\end{aligned} \tag{B7}$$

APPENDIX C: TYPOS CORRECTIONS IN THE ZHDANOV MONOGRAPH

Here, we provide corrections to mistakes found in the eighth chapter of the original monograph.[1]

Note, in this Appendix C, the temperature is given in Kelvin following the system of units used in Ref. 1.

In the expressions (8.1.4), the numerator in the second term has to be changed. The correct numerator is 136, not 139,

$$G^{(11)}_{\alpha Z\beta\zeta} = -\left(\frac{433}{280}\frac{m^2_\beta}{m^2_\alpha}+\frac{136}{35}\frac{m_\beta}{m_\alpha}+\frac{459}{35}+\frac{32}{5}\frac{m_\alpha}{m_\beta}+5\frac{m^2_\alpha}{m^2_\beta}\right)\kappa^2_{\alpha\beta}\lambda_{\alpha Z\beta\zeta}. \tag{C1}$$

The coefficient $c^{(5)}_\alpha$ in Eq. (8.4.4) is

$$c^{(5)}_\alpha = \frac{5}{2}\tau^{-1}_\alpha\tau_{\alpha\alpha}\frac{S^{(11)}_\alpha}{S^{(5)}_\alpha S^{(11)}_\alpha - 7(S^{(9)}_\alpha)^2} = \frac{5}{2}\tau^{-1}_\alpha\tau_{\alpha\alpha}\frac{S^{(11)}_\alpha}{D_\alpha}. \tag{C2}$$

The coefficient $c^{(6)}_\alpha$ in Eq. (8.4.4) is

$$c^{(6)}_\alpha = \frac{S^{(8)}_\alpha S^{(9)}_\alpha - S^{(2)}_\alpha S^{(11)}_\alpha}{S^{(5)}_\alpha S^{(11)}_\alpha - 7(S^{(9)}_\alpha)^2} = \frac{S^{(8)}_\alpha S^{(9)}_\alpha - S^{(2)}_\alpha S^{(11)}_\alpha}{D_\alpha}. \tag{C3}$$

Add Boltzmann constant into (8.4.4),

$$\frac{\mathbf{h}_{\alpha z}}{p_{\alpha z}} - \frac{\bar{\mathbf{h}}_\alpha}{p_\alpha} = n_\alpha\tau_\alpha\tau^{-1}_{\alpha\alpha}c^{(5)}_\alpha\left(\frac{\overline{Z^2_\alpha}}{Z^2}k\nabla T_{\alpha z} - k\nabla T_\alpha\right) + c^{(6)}_\alpha(\mathbf{w}_{\alpha z} - \bar{\mathbf{w}}_\alpha), \tag{C4}$$

$$\text{where } \tau^{-1}_\alpha = \sum_\beta\frac{\mu_{\alpha\beta}}{m_\alpha}\tau^{-1}_{\alpha\beta} \quad \text{(the power of } \tau_\alpha \text{ is corrected)}. \tag{C5}$$

Following the analysis given in Ref. 24 and using expressions for the partial bracket integrals provided in Ref. 43, the r.h.s. of (8.1.6') should be changed to

$$\begin{aligned}&-\omega_{\alpha Z}\{\sigma_{\alpha Zlr}e_{slm}k_m\}\\ &\quad=\sum_{\beta,\zeta}\frac{kT}{m_\alpha+m_\beta}\left[\frac{7}{2}kT\mu_{\alpha\beta}\left(\frac{G^{(13)}_{\alpha z\beta\zeta}\pi_{\alpha zrs}}{m^2_\alpha p_{\alpha z}}+\frac{G^{(14)}_{\alpha z\beta\zeta}\pi_{\beta\zeta rs}}{m^2_\beta p_{\beta\zeta}}\right)\right.\\ &\qquad\left.+\frac{G^{(15)}_{\alpha z\beta\zeta}\sigma_{\alpha zrs}}{p_{\alpha z}}+\frac{G^{(16)}_{\alpha z\beta\zeta}\sigma_{\beta\zeta rs}}{p_{\beta\zeta}}\right].\end{aligned} \tag{C6}$$

In Eq. (8.1.7),

$$G^{(14)}_{\alpha Z\beta\zeta} = -\frac{24}{35}\frac{m_\beta}{m_\alpha}\lambda_{\alpha Z\beta\zeta}, \tag{C7}$$

$$G^{(16)}_{\alpha Z\beta\zeta} = \frac{24}{7}\kappa_{\alpha\beta}\frac{m_\beta}{m_\alpha}\lambda_{\alpha Z\beta\zeta}. \tag{C8}$$

DATA AVAILABILITY

The data that support the findings of this study are available from the corresponding author upon reasonable request.

REFERENCES

[1] V. Zhdanov, *Transport Processes in Multicomponent Plasma*, English ed. (Taylor and Francis, London, New York, 2002).
[2] M. Watkins and JET team, "Physics of high performance JET plasmas in DT," Nucl. Fusion **39**, 1227–1244 (1999).
[3] A. Kallenbach, M. Bernert, P. David, M. G. Dunne, R. Dux, E. Fable, R. Fischer, L. Gil, T. Görler, F. Janky, R. M. McDermott, W. Suttrop, G. Tardini, and M. Wischmeier, "Developments towards an ELM-free pedestal radiative cooling scenario using noble gas seeding in ASDEX upgrade," Nucl. Fusion **61**, 016002 (2020).
[4] S. Braginskii, "Transport processes in a plasma," *Reviews of Plasma Physics*, edited by M. A. Leontovich (Consultants Bureau, New York, 1965), p. 1.
[5] H. Grad, "Asymptotic theory of the Boltzmann equation," Phys. Fluids **6**, 147–181 (1963).
[6] V. Zhdanov and P. Yushmanov, "Diffusion and heat transfer in a multicomponent completely ionized plasma," J. Appl. Mech. Tech. Phys. **21**, 453–461 (1980).
[7] A. Bergmann, Y. Igitkhanov, B. Braams, D. Coster, and R. Schneider, "Implementation into B2 of a 21-moment description for the parallel transport," Contrib. Plasma Phys. **36**, 192–196 (1996).
[8] Y. L. Igitkhanov, "Impurity transport at arbitrary densities in the divertor plasma," Contrib. Plasma Phys. **28**, 477–482 (1988).
[9] Y. L. Igitkhanov and A. Runov, "Implication of kinetic effects for fluid codes," Contrib. Plasma Phys. **34**, 221–225 (1994).
[10] R. Schneider, X. Bonnin, K. Borrass, D. Coster, H. Kastelewicz, D. Reiter, V. Rozhansky, and B. Braams, "Plasma edge physics with B2-EIRENE," Contrib. Plasma Phys. **46**, 3–191 (2006).
[11] M. Fichtmüller, G. Corrigan, G. Radford, R. Simonini, J. Spence, and A. Taroni, "Multi-species developments in the EDGE2D code," Contrib. Plasma Phys. **38**, 284–289 (1998).

[12]H. Bufferand, P. Tamain, S. Baschetti, J. Bucalossi, G. Ciraolo, N. Fedorczak, P. Ghendrih, F. Nespoli, F. Schwander, E. Serre, and Y. Marandet, "Three-dimensional modelling of edge multi-component plasma taking into account realistic wall geometry," Nucl. Mater. Energy **18**, 82–86 (2019).
[13]I. Fomin, N. Bobrova, and P. Sasorov, "Transport processes in plasma with an admixture of several heavy impurities," Plasma Phys. Rep. **43**, 621–637 (2017).
[14]P. Helander and D. J. Sigmar, *Collisional Transport in Magnetized Plasmas* (Cambridge University Press, 2005), Vol. 4.
[15]S. Hirshman and D. Sigmar, "Neoclassical transport of impurities in tokamak plasmas," Nucl. Fusion **21**, 1079–1201 (1981).
[16]V. Rozhansky, S. Voskoboynikov, E. Kaveeva, D. Coster, and R. Schneider, "Simulation of tokamak edge plasma including self-consistent electric fields," Nucl. Fusion **41**, 387–401 (2001).
[17]V. Rozhansky, E. Kaveeva, P. Molchanov, I. Veselova, S. Voskoboynikov, D. Coster, G. Counsell, A. Kirk, and S. Lisgo, "New B2SOLPS5.2 transport code for H-mode regimes in tokamaks," Nucl. Fusion **49**, 025007 (2009).
[18]M. Raghunathan, Y. Marandet, H. Bufferand, G. Ciraolo, P. Ghendrih, P. Tamain, and E. Serre, "Generalized collisional fluid theory for multi-component, multi-temperature plasma using the linearized Boltzmann collision operator for scrape-off layer/edge applications," Plasma Phys. Controlled Fusion **63**, 064005 (2021).
[19]S. Wiesen, D. Reiter, V. Kotov, M. Baelmans, W. Dekeyser, A. Kukushkin, S. Lisgo, R. Pitts, V. Rozhansky, G. Saibene, I. Veselova, and S. Voskoboynikov, "The new SOLPS-ITER code package," J. Nucl. Mater. **463**, 480–484 (2015).
[20]X. Bonnin, W. Dekeyser, R. Pitts, D. Coster, S. Voskoboynikov, and S. Wiesen, "Presentation of the new SOLPS-ITER code package for tokamak plasma edge modelling," Plasma Fusion Res. **11**, 1403102 (2016).
[21]E. Sytova, E. Kaveeva, V. Rozhansky, I. Senichenkov, S. Voskoboynikov, D. Coster, X. Bonnin, and R. Pitts, "Impact of a new general form of friction and thermal forces on SOLPS-ITER modelling results," Contrib. Plasma Phys. **58**, 622–628 (2018).
[22]E. Sytova, D. Coster, I. Senichenkov, E. Kaveeva, V. Rozhansky, S. Voskoboynikov, I. Veselova, and X. P. Bonnin, "Derivation of the friction and thermal force for SOLPS-ITER multicomponent plasma modeling," Phys. Plasmas **27**, 082507 (2020).
[23]D. Reiter, M. Baelmans, and P. Börner, "The EIRENE and B2-EIRENE codes," Fusion Sci. Technol. **47**, 172–186 (2005).
[24]V. Zhdanov and A. Stepanenko, "Kinetic theory of transport processes in partially ionized reactive plasma. I. General transport equations," Physica A **446**, 35–53 (2016).
[25]V. Zhdanov and A. Stepanenko, "Kinetic theory of transport processes in partially ionized reactive plasma. II. Electron transport properties," Physica A **461**, 310–324 (2016).
[26]X. Bonnin, D. Coster, O. Wenisch, K. Kukushkin, A. Kukushkin, M. Stanojevic, and S. Voskoboynikov, *SOLPS-ITER User Manual (solps.pdf)* (ITER Organization, 2020).
[27]F. L. Hinton and R. D. Hazeltine, "Theory of plasma transport in toroidal confinement systems," Rev. Mod. Phys. **48**, 239–308 (1976).
[28]W. A. Houlberg, K. C. Shaing, S. P. Hirshman, and M. C. Zarnstorff, "Bootstrap current and neoclassical transport in tokamaks of arbitrary collisionality and aspect ratio," Phys. Plasmas **4**, 3230–3242 (1997).
[29]A. N. Simakov and P. J. Catto, "Drift-ordered fluid equations for field-aligned modes in low-β collisional plasma with equilibrium pressure pedestals," Phys. Plasmas **10**, 4744–4757 (2003).
[30]X. Litaudon, S. Abduallev, M. Abhangi, P. Abreu, M. Afzal, K. Aggarwal, T. Ahlgren, J. Ahn, L. Aho-Mantila, N. Aiba, M. Airila, R. Albanese, V. Aldred, D. Alegre, E. Alessi, P. Aleynikov, A. Alfier, A. Alkseev, M. Allinson, B. Alper, E. Alves, G. Ambrosino, R. Ambrosino, L. Amicucci, V. Amosov, E. A. Sundén, M. Angelone, M. Anghel, C. Angioni, L. Appel, C. Appelbee, P. Arena, M. Ariola, H. Arnichand, S. Arshad, A. Ash, N. Ashikawa, V. Aslanyan, O. Asunta, F. Auriemma, Y. Austin, L. Avotina, M. Axton, and C. Ayres, "Overview of the JET results in support to ITER," Nucl. Fusion **57**, 102001 (2017).
[31]K. Ikeda, "Progress in the ITER physics basis," Nucl. Fusion **47**, E01 (2007).
[32]G. Federici, R. Kemp, D. Ward, C. Bachmann, T. Franke, S. Gonzalez, C. Lowry, M. Gadomska, J. Harman, B. Meszaros, C. Morlock, F. Romanelli, and R. Wenninger, "Overview of EU DEMO design and R&D activities," Fusion Eng. Des. **89**, 882–889 (2014).
[33]Y. Wan, J. Li, Y. Liu, X. Wang, V. Chan, C. Chen, X. Duan, P. Fu, L. Gao, K. Feng, S. Liu, P. Weng, B. Wan, F. Wan, H. Wang, S.-T. Wu, M. Ye, Q. Yang, and Q. Li, "Overview of the present progress and activities on the CFETR," Nucl. Fusion **57**, 102009 (2017).
[34]E. Kaveeva, V. Rozhansky, I. Senichenkov, E. Sytova, I. Veselova, S. Voskoboynikov, X. Bonnin, R. Pitts, A. Kukushkin, S. Wiesen, and D. Coster, "SOLPS-ITER modelling of ITER edge plasma with drifts and currents," Nucl. Fusion **60**, 046019 (2020).
[35]I. Y. Senichenkov, E. G. Kaveeva, E. A. Sytova, V. A. Rozhansky, S. P. Voskoboynikov, I. Y. Veselova, A. S. Kukushkin, D. P. Coster, F. Reimold, X. Bonnin, and ASDEX-upgrade team, "Study of detached H-modes in full tungsten ASDEX upgrade with N seeding by SOLPS-ITER modeling," in Proceedings of the 24th IAEA Fusion Energy Conference, 2018.
[36]E. Sytova, R. A. Pitts, E. Kaveeva, X. Bonnin, D. Coster, V. Rozhansky, I. Senichenkov, I. Veselova, S. Voskoboynikov, and F. Reimold, "Comparing N versus Ne as divertor radiators in ASDEX-upgrade and ITER," Nucl. Mater. Energy **19**, 72–78 (2019).
[37]D. S. Sorokina, I. Y. Senichenkov, V. A. Rozhansky, and E. O. Vekshina, "Modeling of globus-m2 spherical tokamak edge with nitrogen seeding," Phys. Plasmas **25**, 122514 (2018).
[38]I. Y. Senichenkov, E. G. Kaveeva, E. A. Sytova, V. A. Rozhansky, S. P. Voskoboynikov, I. Y. Veselova, D. P. Coster, X. Bonnin, F. Reimold, and ASDEX-upgrade team, "On mechanisms of impurity leakage and retention in the tokamak divertor," Plasma Phys. Controlled Fusion **61**, 045013 (2019).
[39]A. Kukushkin, H. Pacher, V. Kotov, G. Pacher, and D. Reiter, "Finalizing the ITER divertor design: The key role of SOLPS modeling," Fusion Eng. Des. **86**, 2865–2873 (2011).
[40]H. Bufferand, C. Baudoin, J. Bucalossi, G. Ciraolo, J. Denis, N. Fedorczak, D. Galassi, P. Ghendrih, R. Leybros, Y. Marandet, N. Mellet, J. Morales, N. Nace, E. Serre, P. Tamain, and M. Valentinuzzi, "Implementation of drift velocities and currents in SOLEDGE2D-EIRENE," Nucl. Mater. Energy **12**, 852–857 (2017).
[41]Y. Feng, F. Sardei, J. Kisslinger, P. Grigull, K. McCormick, and D. Reiter, "3d edge modeling and island divertor physics," Contrib. Plasma Phys. **44**, 57–69 (2004).
[42]B. Viola, G. Calabró, A. Jaervinen, I. Lupelli, F. Maviglia, S. Wiesen, M. Wischmeier, and J. Contributors, "EDGE2D-EIRENE simulations of the impact of poloidal flux expansion on the radiative divertor performance in JET," Nucl. Mater. Energy **12**, 786–790 (2017).
[43]L. Woods, "Mathematical theory of transport processes in gases. by J. H. Ferziger and H. G. Kaper. North-Holland, 1972. 579 pp. H£1.120," J. Fluid Mech. **61**, 823–825 (1973).